Department of Equine and Small Animal Medicine,
Faculty of Veterinary Medicine,
University of Helsinki

Contrast-enhanced ultrasound of abdominal organs in cats

Merja Leinonen

ACADEMIC DISSERTATION

To be presented, with permission of the Faculty of Veterinary Medicine,
University of Helsinki, for public examination in Auditorium XIV,
University Main Building,
on March 11th 2011, at 12 noon.

Helsinki 2011

SUPERVISED BY:
Marja Raekallio, DVM, PhD, University Lecturer
Outi Vainio, DVM, PhD, Dipl. ECVPT, Professor
Mirja Ruohoniemi, DVM, PhD, CertVR, Dipl.ECVDI, University Lecturer
Department of Equine and Small Animal Medicine
Faculty of Veterinary Medicine
University of Helsinki
Helsinki, Finland

In co-operation with:
Robert T. O'Brien, DVM, MSc, Dipl. ACVR, Professor
Department of Clinical Medicine
University of Illinois at Urbana-Champaign
Urbana, Illinois, USA

REVIEWED BY:
Jimmy Saunders DVM, PhD, Dipl. ECVDI, Associate Professor
Department of Veterinary Medical Imaging and Small Animal Orthopaedics
Faculty of Veterinary Medicine
University of Ghent
Ghent, Belgium
Dominique Pennick DVM, PhD, Dipl. ECVDI/ACVR, Professor
Section of Radiology
Department of Surgery
Cummings School of Veterinary Medicine
Tufts University
Grafton, Massachusetts, USA

OPPONENT:
Fintan McEvoy, MVB, PhD, DVR, Dipl. ECVDI, MRCVS, Professor
Department of Small Animal Clinical Sciences
University of Copenhagen
Denmark

Cover (ultrasound images embedded in a cat figure) contrast-enhanced ultrasound images of cat liver, spleen, kidney, pancreas, small intestine and mesenteric lymph nodes
ISBN 978-952-92-8583-9 (pbk.)
ISBN 978-952-10-6814-0 (PDF)
Unigrafia oy, Helsinki University Printing House
Helsinki 2011
Http://ethesis.helsinki.fi

Abstract

The primary aim of this thesis was the evaluation of the perfusion of normal organs in cats using contrast-enhanced ultrasound (CEUS), to serve as a reference for later clinical studies. Little is known of the use of CEUS in cats, especially regarding its safety and the effects of anesthesia on the procedure, thus, secondary aims here were to validate the quantitative analysing method, to investigate the biological effects of CEUS on feline kidneys, and to assess the effect of anesthesia on splenic perfusion in cats undergoing CEUS.

The studies were conducted on healthy, young, purpose-bred cats. CEUS of the liver, left kidney, spleen, pancreas, small intestine, and mesenteric lymph nodes was performed to characterize the normal perfusion of these organs on ten anesthetized, male cats. To validate the quantification method, the effects of placement and size of the region of interest (ROI) on perfusion parameters were investigated using CEUS: Three separate sets of ROIs were placed in the kidney cortex, varying in location, size, or depth. The biological effects of CEUS on feline kidneys were estimated by measuring urinary enzymatic activities, analyzing urinary specific gravity, pH, protein, creatinine, albumin, and sediment, and measuring plasma urea and creatinine concentrations before and after CEUS. Finally, the impact of anesthesia on contrast enhancement of the spleen was investigated by imaging cats with CEUS first awake and later under anesthesia on separate days.

Typical perfusion patterns were found for each of the studied organs. The liver had a gradual and more heterogeneous perfusion pattern due to its dual blood flow and close proximity to the diaphragm. An obvious and statistically significant difference emerged in the perfusion between the kidney cortex and medulla. Enhancement in the spleen was very heterogeneous at the beginning of imaging, indicating focal dissimilarities in perfusion. No significant differences emerged in the perfusion parameters between the pancreas, small intestine, and mesenteric lymph nodes.

The ROI placement and size were found to have an influence on the quantitative measurements of CEUS. Increasing the depth or the size of the ROI decreased the peak intensity value significantly, suggesting that where and how the ROI is placed does matter in quantitative analyses.

A significant increase occurred in the urinary N-acetyl-β-D-glucosaminidase (NAG) to creatinine ratio after CEUS. No changes were noted in the serum biochemistry profile after CEUS, with the exception of a small decrease in blood urea concentration. The magnitude of the rise in the NAG/creatinine ratio was, however, less than the circadian variation reported earlier in healthy cats. Thus, the changes observed in the laboratory values after CEUS of the left kidney did not indicate any detrimental effects in kidneys.

Heterogeneity of the spleen was observed to be less and time of first contrast appearance earlier in nonanesthetized cats than in anesthetized ones, suggesting that anesthesia increases heterogeneity of the feline spleen in CEUS.

In conclusion, the results suggest that CEUS can be used also in feline veterinary patients as an additional diagnostics aid. The perfusion patterns found in the imaged organs were typical and similar to those seen earlier in other species, with the exception of

the heterogeneous perfusion pattern in the cat spleen. Differences in the perfusion between organs corresponded with physiology. Based on the results, estimation of focal perfusion defects of the spleen in cats should be performed with caution and after the disappearance of the initial heterogeneity, especially in anesthetized or sedated cats. Finally, these results indicate that CEUS can be used safely to analyze kidney perfusion also in cats.

Future clinical studies are needed to evaluate the full potential of CEUS in feline medicine as a tool for diagnosing lesions in various organ systems.

Contents

Acknowledgments

This study was carried out at the Department of Equine and Small Animal Medicine, Faculty of Veterinary Medicine, University of Helsinki and the practical work was performed at the Department of Clinical Sciences, Kansas State University (KSU), USA, and the Department of Clinical Medicine, University of Illinois (UIUC), USA, from 2007 to 2010.
Financial support provided by the Faculty of Veterinary Medicine, the Finnish Veterinary Foundation, the Helvi Knuuttila Trust, and the Orion-Farmos Research Foundation is gratefully acknowledged.

I owe my deepest gratitude to the following persons:

- Professor Robert T. O'Brien for inspiring ideas, co-operation, and practical advice throughout the study and for giving me the opportunity to work with him.
- My supervisors: Docent Marja Raekallio, Professor Outi Vainio, and Docent Mirja Ruohoniemi for their support and commitment, excellent supervision, endless encouragement, valuable guidance, practical advice, helpful and inspiring ideas and suggestions, and seemingly endless revisions!

Without the help of my co-authors this work could not have been done. I warmly thank:

- Professor David S. Biller
- Satu Sankari

Over the years, several people have been involved in this project, and I sincerely thank everyone for their contribution. The following persons are especially acknowledged:

- Professor Marjatta Snellman for support in both radiology and life in general and for introducing me to foreign collaborators, you have been the mother of my radiological studies!
- Associate Professor Hannu Rita for statistical help
- Laboratory technician Mari Palviainen for help with laboratory measurements
- Other staff members (KSU, UIUC), especially Cintia Ribeiro de Oliveira and Tonya Keel Ridge (UIUC), for helping in handling the cats throughout the study
- Carol Ann Pelli for editing the language of the thesis
- Pia Virtanen for help with illustrations and cover
- Niko Helle for the photography in back cover
- Kristian Lindqvist for technical and computer help and for assistance with tables and illustrations
- for all my friends that helped me with finalizing the reference list

I am grateful to Associate Professor Jimmy Saunders DVM, PhD, Dipl. ECVDI, and Professor Dominique Pennick DVM, PhD, Dipl. ECVDI/ACVR, for reviewing the manuscript of this dissertation, and for their constructive criticism, valuable corrections and suggestions that improved the final version of this dissertation. I am also very grateful for Associate Professor Fintan McEvoy MVB, PhD, DVR, DipECVDI, MRCVS, for accepting the role of opponent.

And last, but not least, my sincere thanks to my family, especially my mother for all the sacrifices she made for my education and for the love and care always generously provided. This PhD would never have been completed without her help and support.

I dedicate this work to my father who encouraged and inspired me to evolve as a person, a veterinarian, and a scientist.

1. List of original publications

This thesis is based on the following original articles that are referred to in the text by their Roman numerals:

I Leinonen, M.R., Raekallio, M.R., Vainio, O.M., Ruohoniemi, M.O., Biller, D.S., O'Brien, R.T. (2010) Quantitative analysis of the perfusion in the kidneys, liver, pancreas, small intestine and mesenteric lymph nodes in healthy cats using contrast-enhanced ultrasound. American Journal of Veterinary Research 71(11), 1305-1311.

II Leinonen, M.R., Raekallio, M.R., Vainio, O.M., Ruohoniemi, M.O., O'Brien, R.T. (2011) The effect of the sample size and location on contrast ultrasound measurements of perfusion. Veterinary Radiology & Ultrasound, 52(1), 82-87.

III Leinonen, M.R., Raekallio, M.R., Vainio, O.M., Sankari, S., O'Brien, R.T. (2010) The effect of contrast ultrasound on kidneys of eight cats. The Veterinary Journal, in press: DOI information: 10.1016/j.tvjl.2010.09.007.

IV Leinonen, M.R., Raekallio, M.R., Vainio, O.M., O'Brien, R.T. (2010) Effect of anesthesia on contrast-enhanced ultrasound of the feline spleen. The Veterinary Journal, in press: DOI information:10.1016/j.tvjl.2010.10.013.

 In addition, some unpublished material has been presented.

2. Abbreviations

ACP	Acid phosphatase
AKI	Acute kidney injury
ALP	Alkaline phosphatase
ALT	Alanine-aminotransferase
AST	Aspartate aminotransferase
AT	Arrival time
AT_v	Arrival time estimated visually
BI	Baseline intensity
BUN	Blood urea nitrogen
CEUS	Contrast-enhanced ultrasound
CO	Cardiac output
FNA	Fine needle aspiration
GGT	Gamma-glutamyl transferase
Hb	Hemoglobin
Hct	Hematocrit
hpf	High power field
HR	Heart rate
im	Intra-muscular(ly)
iv	Intra-venous(ly)
LDH	Lactate dehydrogenase
MAP	Mean arterial pressure
MCH	Mean cell hemoglobin
MCV	Mean cell volume
MI	Mechanical index
NAG	N-acetyl-β-D-glucosaminidase
PI	Peak intensity
Plt	Platelet count
RBC	Red blood cell
ROI	Region of interest
Sp	Specific gravity
sc	sub-cutaneous(ly)
SVR	Systemic vascular resistance
TIC	Time-intensity curve
$TTHe_{inj}$	Time to heterogeneity from injection
$TTHo_{inj}$	Time to reach homogeneity from injection
TTP_{inj}	Time to peak from injection
TTP_{inr}	Time to peak from initial rise
USCA	Ultrasound contrast agent
WBC	White blood cell
Wi	Wash-in rate
Wo	Wash-out rate

3. Introduction

Ultrasonography has been commonly used in veterinary medicine to image the architecture of abdominal organs. Ultrasound is considered a good, easy to perform and non-invasive imaging modality in diagnosing various diseases. Blood scatters poorly compared with tissues in conventional ultrasound. Therefore, Doppler techniques have been used to analyze blood flow (Rubin et al., 1994). However, Doppler cannot detect flow of a low volume or velocity, or flow from unfavorable angles or in deep tissues (Rubin et al., 1994; Taylor et al., 1996; Nilsson et al., 1997). Furthermore, Doppler is very sensitive to motion artifacts, making it sometimes difficult to use with awake or panting animals. The scattering ability of the blood can be enhanced with gas-containing microbubbles called ultrasound contrast agents (USCAs). Contrast-enhanced ultrasound (CEUS) is free from the above-mentioned restrictions of Doppler imaging and even very small vessels, such as capillary level microcirculation, can be detected (Greis, 2004).

CT and MRI have long been the golden standard for imaging malignancies in human medicine (Villa et al., 1995). The possible side-effects, including adverse or allergic reactions and potential nephrotoxicity of these iodine- and gadolinium-containing contrast agents, limit their use particularly in patients with kidney disease (Mehran et al., 2006; Persson et al., 2006; Perazella, 2008). The use of CT and MRI for evaluation of masses and tumors has been studied to a certain extent in veterinary medicine (Le Blanc et al., 2007; Ohlerth et al., 2007b). However, detailed studies from specific CT or MRI changes in abdominal organs with numerous disease processes are still lacking. In addition to the possible toxicities of CT and MRI contrast agents, the need for anesthesia further limits the use of both CT and MRI in veterinary patients.

CEUS is based on highly reflecting microbubbles that give contrast between the surrounding tissues and blood (Calliada et al., 1998). The echoes from the blood are normally too low to be detected with basic ultrasound and appear anechoic in relation to the surrounding hypoechoic soft tissues. With USCAs, the echoes returning from the blood are enhanced so that even tissue parenchymal microcirculation can be detected. For the detection of real-,time perfusion in the tissues, a specialized contrast-specific ultrasound technique (eg. harmonic and coded imaging or phase amplitude modulation) is needed to visualize returning echoes from the microbubbles/blood, allowing detection of tissue microcirculation (Calliada et al., 1998). Contrast agents are therefore useful for more accurate detection and characterization of many intra-abdominal diseases, including liver nodules, kidney lesions, metastases, trauma and infarction.

CEUS was first introduced to human medicine as a new method for detecting congenital cardiac defects (Drobac et al., 1983) and detecting and characterizing focal changes in the liver (Nicolau et al., 2004). Nowadays, CEUS is used for more detailed detection and characterization of focal changes in perfusion in various organs, including the spleen (Görg et al., 2007), kidneys (Bertolotto et al., 2008), pancreas (D'Onofrio et al., 2007), prostate (Karaman et al., 2005), mammary gland (Chaudhari et al., 2000), adrenals (Friedrich-Rust et al., 2008), and lymph nodes (Bude, 2004). Liver lesions can be diagnosed with high accuracy as benign or malignant with CEUS (Nicolau et al., 2004; Lee, 2005).

CEUS has been proven to be a safe and minimally invasive diagnostic tool for human (Blomley et al., 2007; Piscaglia et al., 2006) and veterinary (Ziegler et al., 2003; Nyman et al., 2005; Rademacher et al., 2008) patients. The only current accepted clinical indication for using contrast ultrasound in veterinary medicine is the detection and characterization of lesions in the liver, spleen, and lymph nodes in dogs (O'Brien et al., 2004a; Salwei et al., 2005; Kutara et al., 2006; O'Brien, 2007; Ohlerth et al., 2008; Rossi et al., 2008; Ivancic et al., 2009). The lack of baseline studies and limited knowledge about the effect of anesthesia on CEUS, and the behavior of USCAs in cats, including possible harmful effects on kidney function, have restricted the use of the tool for clinical feline patients.

The aim of this thesis is to provide evidence-based knowledge of the use of CEUS in cats, and to serve as a background for future clinical studies. The use of CEUS is expected to widen the diagnostic possibilities in veterinary medicine.

3. Review of the literature

3.1. Contrast-enhanced ultrasound (CEUS)

CEUS is based on enhancing the returning echoes from the blood by USCAs over the tissue backscattering. Both the sensitivity and specificity of ultrasound imaging can be increased with USCAs. An increase in the signal intensity can be detected in conventional B-mode ultrasound as a slight image enhancement (Uhlendorf, 1994; Bouakaz et al., 1998). The contrast enhancement is detected even better for a brief moment with Doppler imaging or in real time with contrast-specific detection modes (Frush et al., 1995). The Doppler-method is today used mainly in transcranial imaging to improve the signal-to-noise ratio, when the ultrasound signal is attenuated by the skull (Seidel et al., 2000; Seidel et al., 2009). Most of the CEUS studies are currently performed utilizing contrast-specific software. These techniques exploit the specific acoustic properties of USCA microbubbles and enable continuous real-time imaging of tissue parenchymal blood flow, by suppressing signals from tissues, and thus, intensifying the signals from USCAs (de Jong et al., 2001).

3.1.1. Signal processing

Contrast-specific software is based on suppressing the signals from the background tissues and enhancing the signals from the microbubbles, giving good contrast between the blood and tissue. Several techniques have been developed for signal processing to selectively collect information from the non-linear microbubble oscillations; these include second harmonic imaging (Schrope et al., 1993), pulse inversion harmonic imaging (Simpson et al., 1999), and cadence-contrast pulse sequencing and power (amplitude) modulation (de Jong et al., 2001; Thomas et al., 2009).

The behavior of microbubbles is affected by ultrasound scanning parameters, such as resonance frequency, pulse repetition frequency, number and location of focal zones, and acoustic power, and by the properities of the filling gas, damping coefficients, and shell properties (de Jong et al., 1994a; 1994b; Hoff, 1996; Moran et al., 1998; Hoff et al., 2000; Uhlendorf et al., 2000; de Jong et al., 2002; Emmer et al., 2007; Whittingham et al., 2007; Yeh et al., 2008). Local acoustic power is the principal parameter directing the behavior of microbubbles (Emmer et al., 2007; Yeh et al., 2008). The local acoustic power depends mainly on the output power of the ultrasound system, the transmission frequency, and the attenuation of the ultrasound beam with depth (Whittingham et al., 2007; Yeh et al., 2008). Depending on the acoustic power, different interactions between the incident ultrasound beam and the microbubbles take place, including scattering, resonance and microbubble destruction (de Jong et al., 1994a; 1994b; Raichlen, 2001; Sboros et al., 2003; Emmer et al., 2007; de Jong et al., 2007).

The output power combined with transmit frequency is reflected by the mechanical index (MI), which originally measured the potential for mechanical damage to tissues

exposed to ultrasound pulses (Raichlen, 2001; Bouakaz et al., 2007). MI also gives an indication of the likelihood of bubble destruction: the higher the MI, the greater its destructive properties and the poorer the contrast effects (Raichlen, 2001; de Jong et al., 2002). However, these parameters are not directly comparable between different ultrasound systems because of differences in technology of ultrasound equipment and companies.

Contrast-specific detection modes utilize the interaction of the microbubbles with ultrasound waves. This interaction depends on microbubble size, shell flexibility, transducer frequency, and MI (Church et al., 1995; Frinking et al., 1998; de Jong et al., 2000; Uhlendorf et al., 2000; Bouakaz et al., 2007; Emmer et al., 2007; van der Meer et al., 2007; Yeh et al., 2008). At very low acoustic power the oscillation is symmetrical and the change in size is equal in both compression and expansion (Uhlendorf, 1994; van Liew et al., 1995; Hoff, 1996). When acoustic power is increased, the bubbles start to expand more than compress, and thus, the oscillations become asymmetric (Hoff, 1996). These asymmetric signals emitted by microbubbles can be detected at transmitted (fundamental) ultrasound frequency and at multiples of this frequency, e.g. the second harmonic at double the transmitted frequency (de Jong et al., 1994a; 1994b).

This separation of harmonic microbubble signals from the fundamental linear signals arising from tissue results in loss of image resolution. Furthermore, the tissues can also produce harmonic signals with use of high acoustic power (Dong et al., 1999; Uhlendorf et al., 2000). Distinguishing between tissue and microbubble harmonic signals is challenging even with contrast-specific detection modes. However, the newer, second- and third generation microbubbles with an elastic shell can be made to oscillate asymmetrically with very low acoustic powers, enabling the separation of microbubble and tissue harmonics and a reduced signal-to-noise ratio (Ward et al., 1997; Wu et al., 1998; Uhlendorf et al., 2000). Furthermore, with low acoustic power (low MI), real time scanning is made possible, allowing dynamic perfusion studies.

3.1.2. Use in human medicine

CEUS is used in human medicine for more detailed detection and characterization of focal changes in perfusion in several organs, including the heart (Kitzman et al., 2000), liver (Nicolau et al., 2004), spleen (Görg et al., 2007), kidneys (Nilsson, 2004), pancreas (Kitano et al., 2004), prostate (Karaman et al., 2005), mammary gland (Chaudhari et al. 2000), adrenals (Friedrich-Rust et al., 2008), and lymph nodes (Bude, 2004). It is also used in detecting pathological changes affecting large vessels and in diagnosing abdominal trauma (Leen et al., 2004; Martegani et al., 2004; Thorelius, 2004). CEUS is not only important in detecting the aforementioned perfusional changes and aiding diagnostic work in suspicion of neoplastic, traumatic, or necrotic lesions, but also in the treatment and monitoring of cancer (Leen et al., 2004; Solbiati et al., 2004). Most studies have, however, been focused on the liver. Because of the dual blood flow in the liver, the differentiation of liver lesions as benign or malignant can be made with high accuracy with the help of CEUS, even up to the histological level (Nicolau et al., 2004; Lee, 2005; Claudon et al., 2008).

3.1.3. Use in veterinary medicine

In veterinary medicine, CEUS is currently indicated for clinical use in the detection and characterization of lesions in the liver, spleen, prostate, and lymph nodes, and in detection of kidney infarctions and lesions in dogs (O'Brien et al., 2004a; Salwei et al., 2005; Kutara et al., 2006; Ohlerth et al., 2008; Rossi et al., 2008; 2010; Ivancic et al., 2009; Kanemoto et al., 2009; Nakamura et al., 2009; 2010; Haers et al., 2010; Vignoli et al., 2010). For example, in the liver malignant tumors enhance early with CEUS due to mainly arterial blood flow, whereas benign tumors are usually uniformly isoechoic relative to the surrounding liver (O'Brien et al., 2004a). In other organs, such as the kidneys and spleen, lesions are mainly classified as hyper-, iso-, or hypovascular, based on how they enhance in relation to the surrounding parenchymal tissue (Ohlerth et al., 2008; Haers et al., 2010). The diagnostic possibilities of CEUS in veterinary medicine are constantly increasing. Studies are available of CEUS of the pancreas, adrenal gland, and testicles (Johnson-Neitman et al. 2007; Pey et al., 2010; Volta et al., 2010). However, no studies have been reported of diffuse organ diseases and CEUS in veterinary medicine, and only a few in human medicine (Rahbin et al., 2008, Li et al., 2010). Several studies have been conducted with healthy dogs to investigate normal perfusion in various organs (liver, spleen, kidneys, prostate, stomach, small intestine) (Ziegler et al., 2003; Nyman et al., 2005; Kamino et al., 2006; Ohlerth et al., 2007a; Waller et al., 2007; Nakamura et al., 2009, Russo et al., 2009; Vignoli et al. 2010; Bigliardi et al., 2011; Jiménez et al., 2011), but little is known about the effect of anesthesia on CEUS (Nyman et al., 2005). In cats, however, only a few studies have been published on the use of CEUS; in evaluating the normal perfusion of kidneys in healthy cats (Kinns et al., 2010) and in diagnosing pancreatic disease using contrast-enhanced power and color Doppler techniques (Rademacher et al., 2008).

3.1.4. Quantification of perfusion

In CEUS, the perfusion of a tissue or organ is assessed quantitatively from time-intensity curves (TICs) in a selected region of interest (ROI). The shape of the TIC has been shown to reflect the vascular structure of the imaged organ (Li et al., 2006; Metoki et al., 2006). Therefore, the tissue perfusion can be estimated with CEUS, as concentration of microbubbles in blood flow (signal intensity), indicating quantity of blood flow (Wei, 2001; Lucidarme et al., 2003). In quantitative analyses, detailed information of signal intensity vs. time can be obtained from a selected ROI, resulting in several perfusion parameters, such as contrast arrival time (AT), time to peak intensity (TTP_{inj}), and peak intensity (PI), acquired from the generated TIC (Du et al., 2008; Fleischer et al., 2008). The size and location of an ROI have been shown to have an effect on the intensity values obtained in experimental and theoretical models (Claudon et al., 1999; Taylor et al., 1999; Schlosser et al., 2001; Sonne et al., 2003; Mulé et al., 2008). The main clinical use of perfusion parameters is assessment of blood flow changes in an organ or tissue in real-time (Quaia et al., 2006). This aids in distinguishing between normal and abnormal flow, thereby facilitating characterization of the pathology.

The relationship between microbubble concentration and signal intensity has been found to vary depending on the concentration (Taylor et al., 1996; Forsberg et al., 2001; Wei, 2001; Li et al. 2005). The relationship between bubble concentration and signal intensity is linear with low microbubble concentrations, becoming exponential with higher concentrations (Skyba et al., 1994; Forsberg et al., 2001). Besides microbubble concentration, the size of the activated microbubbles in the circulation has an effect on the intensity detected (Porter et al., 1997; Emmer et al., 2007; Goertz et al., 2007). Unfortunately, several other factors can impair accurate perfusion quantification, the most important of which are motion artifact and shadowing effect resulting from signal intensity attenuation caused by microbubbles (Li et al., 2006; Mulé et al., 2007). Motion artifact can be detected in the image as local changes in signal intensity with replenishment of microbubbles or movement of the ROI outside the targeted tissue. Motion artifact can also be seen in the TIC as false peaks and troughs. For an accurate quantification of perfusion, motion artifact needs to be taken into account and removed before analyses. Attenuation can be seen in the image as decreased signal intensity in the far-field either quantitatively or, if high enough, visually.

Besides having a direct impact on perfusion quantification by influencing microbubble backscattering, microbubble concentration has an effect on the attenuation of the ultrasound (Porter et al., 1997; Forsberg et al., 2001; Li et al., 2005). For quantitative measurements, sufficiently low microbubble concentrations, i.e. a linear relationship between microbubble and signal intensity, are needed (Forsberg et al., 2001; Wei, 2001; Rognin et al., 2008). When the concentration exceeds this, the tissue signal intensity starts to approach the signal intensity of a blood pool such as large vessels, and the relationship becomes exponential (Wei, 2001). Microbubble saturation must therefore be avoided to enable quantification (Wei, 2001; Li et al., 2005; Rognin et al., 2008). However, there are also multiple other factors influencing the attenuation in CEUS in vivo, such as bubble size and shell type (Emmer et al., 2007), acoustic pressure (Emmer et al., 2007; 2009), and transducer frequency (Yeh et al., 2008), making image optimization challenging. Furthermore, bubble size and behavior have been reported to change with varying injection techniques (Talu et al., 2008; Kaya et al., 2009), vessel type and size (Qin et al., 2007), tissue temperature (Mulvana et al., 2010), and over time (Goertz et al., 2007).

Whether bolus injection technique or constant infusion is better for quantifying perfusion is under debate (Wei, 2001; Okada et al., 2005; Kaya et al., 2009; Su et al., 2009). Contrast enhancement has been reported to last longer, but to be less marked with the infusion technique (Okada et al., 2005). However, no difference appeared in the lesion to liver contrast between the two techniques in a previous study (Okada et al., 2005). Due to less intense enhancement with infusion, less attenuation can be expected in the far-field of the image, and it may also be customized with titrating the USCA dose (Wei, 2001). On the other hand, changes in the spatial distribution of the microbubbles have been reported with the infusion technique without specific mixing devices over time (Kaya et al., 2009). Furthermore, the different enhancement phases in the liver are not detected with infusion, and thus, dynamic lesion characterization can be impaired, especially with hypervascular lesions (Okada et al., 2005).

3.2. Ultrasound contrast agents (USCAs)

3.2.1. Physical properties of USCAs

The development of USCAs began decades ago, after an incidental finding during echocardiographic examination, when saline was injected intra-cardially in a human patient and an enhancement of the ultrasound signal was observed during the injection due to air bubbles within the saline (Gramiak et al., 1968). Since then, developments in USCAs have been dramatic. The future of USCAs is in molecular-level imaging, targeted CEUS, and drug delivery.

USCAs consist of gas-filled microbubbles encapsulated by a shell of different composition. The gas inside the microbubbles is stable, low-soluble, biologically inert, and non-toxic (Lester at al., 1950; Morel et al., 2000; FDA, 2001; EMEA, 2005; Bouakaz et al., 2007). The size of the microbubbles corresponds to the size of red blood cells (2-8 μm). Microbubbles are therefore big enough (high molecular weight) not to diffuse to the extracellular space, but small enough to pass the lung capillary system without being filtered out of the body system (Morel et al., 2000; Wheatley, 2001; Bouakaz et al., 2007). The size of the microbubbles is smaller than the ultrasound beam wavelength, and therefore, microbubbles behave as scattering reflectors. The large difference in acoustic impedance between the gas-containing microbubbles and the surrounding fluid (blood) improves the scattering reflector ability of the microbubbles (Cosgrove, 1997; Arditi et al., 1997; Moran et al., 2000; Frinking et al., 2001; de Jong et al., 2002). These special properties of the microbubbles keep them unchanged in cardio-pulmonary circulation (Morel et al., 2000; Bouakaz et al., 2007), producing a marked increase (75%) in image contrast and systemic enhancement of macro- and microvasculature relative to basic non-contrast-ultrasound (Pace et al., 1997; Girard et al., 2000).

USCAs are mainly administered intravenously (iv), although they can be used as a direct injection as well, e.g. into the urinary bladder to detect ureteral reflux (Darge et al., 2002). After an iv administration, microbubbles stay actively within the vascular compartment for several minutes (Morel et al., 2000). In general, microbubbles do not cross the endothelium, unlike contrast agents used in CT- and MRI studies, and therefore, USCAs are considered true blood pool agents (Bauer et al., 2003; Greis, 2004). A previously used USCA, Levovist®, however, stayed in the liver and spleen parenchyma longer than expected, yielding a late parenchymal enhancement phase (Blomley et al., 1998; Leen, 2001; Quaia et al., 2002). Some of the second-generation contrast agents (Sonazoid®, Sonavist®) have similar effects, giving a late parenchymal enhancement phase possibly due to selective uptake by reticuloendothelial Kupffer cells in the liver (Leen, 2001; Lim et al., 2004; Yanagisawa et al., 2007). It can, therefore, be debated whether these agents are pure blood pool agents or not.

The gas component used in microbubbles is often a high molecular weight gas, because of the low solubility (slow diffusion rate) and long persistence of microbubbles, diminishing the amount of gas needed and providing a longer effective life for the microbubbles in circulation (Uhlendorf et al., 2000; Bouakaz et al., 2007). The most commonly used gas-types in the newer, second-generation USCAs are perfluoro gases,

e.g. perfluorocarbons like perfluoropropane used in Definity®, or sulfur hexafluoride in Sonovue® (Package leaflet; FDA, 2001; EPAR, 2008). Both of these contrast agents provide strong enhancement and have excellent durability (Moran et al., 2000; 2002).

The shell in the microbubbles can consist of various chemical compositions. They can be phospholipid (Definity®, Sonovue®) (Arditi et al., 1997; Rosenberg et al., 2002), polymeric (biopolymers, proteins) (Wheatley et al., 1990), non-ionic surfactants (Forsberg et al., 1997) or galactose-based (Albrecht et al., 2000; Wheatley, 2001). The main purpose of the shell is to stabilize the microbubble (Frinking et al., 1998; Moran et al., 1998; Bouakaz et al., 2007). It also has an effect on acoustic behavior and fate (Frinking et al., 1998; Bouakaz et al., 2007; de Jong et al., 2009). For harmonic imaging, the shell needs to be flexible enough to allow the size of the microbubbles to change during oscillation, while also being stable enough to act as a protective shield, preventing microbubble breakage and allowing the microbubbles to circulate several times through the whole blood volume (Bouakaz et al., 2007). For the detection of liver tumors, uptake by the reticuloendothelial system is useful, and more rigid shells are needed (Wheatley, 2001).

3.2.2. Microbubble behavior

Microbubbles are modified by the ultrasound process (Uhlendorf et al., 2000). The size of the microbubbles changes in interaction with the ultrasound waves, making bubbles oscillate (Uhlendorf et al., 2000). The response of the microbubbles depends mainly on insonation (Moran et al., 2000; Emmer et al., 2007), which can roughly be estimated by MI. At a low acoustic power (low MI: ≈0.1-0.2), the microbubbles are stable and act as reflectors (Whittingham et al., 2007). At a medium acoustic power microbubbles start to oscillate (Chomas et al. 2002; Cosgrove, 2006). When the acoustic power (acoustic pressure) is high (MI: >0.7), and the oscillations become very strong, the microbubbles rupture (Frinking et al., 1998; Bouakaz et al., 2005; Miller et al., 2007).

Oscillation ability enables the use of microbubbles with a high range of ultrasound frequencies (1.7–50 MHz) (Greis, 2004; Goertz et al., 2007). Microbubble size and stability therefore have an influence on the selected transducer frequency and the type used (Gorce et al., 2000; Emmer et al., 2007; Goertz et al., 2007). The size of the bubbles is not constant (Emmer et al., 2007; Goertz et al., 2007). Each ultrasound contrast agent has its own reference range for the size of the microbubble (Definity®: 1-3 μm, Sonovue®: 1-10 μm), which is stated in the manufacturer's information.

3.3. Vascular anatomy and physiology of abdominal organs

CEUS can be used to estimate organ perfusion, either to quantitate it or to detect focal perfusional changes. To be able to fully understand the perfusion quantification and the relationship in the perfusion between various abdominal organs, knowledge of vascular anatomy and physiology is essential. In the following sections, vascular anatomy of the

abdominal organs studied will be briefly discussed. In veterinary medicine, the cat is typically assumed to have a similar anatomy and physiology as the dog or other species. The vascular anatomy of larger abdominal vessels, such as the aorta, vena cava caudalis, and portal vein, and their branches, is known in the cat. However, the microvascular anatomy and physiology are not well known. Most of the studies concerning vascular physiology and microvascular anatomy have been performed with laboratory animals other than the dog and cat. The following sections refer mostly to the microvascular anatomy of the dog or humans, with a few exceptions, which are indicated in the text. In general, we assume that the anatomy follows the same principles, unless otherwise mentioned.

3.3.1. Liver

The liver is supplied by the hepatic artery (20%), which branches from the celiac artery, and portal vein (80%), which drains blood from the cranial and caudal mesenteric, splenic, and gastroduodenal veins. The hepatic artery divides further into 3-5 branches at the hilus of the liver. These branches supply accordingly the right liver lobes (lateral, medial, caudate), parts of the right medial, quadrate, and left medial lobes, and parts of the left medial and quadrate lobes and the entire left lateral lobe. The portal vein branches after the liver hilus into 2-3 branches: the right, middle, and left portal branch. The portal veins and hepatic arteries run in parallel in the liver, branching repeatedly. The terminal branches, portal venules, and hepatic arterioles supply blood into the hepatic sinusoids, where they partially anastomose. The blood from the sinusoids is collected in central venules draining into the hepatic veins and vena cava (Schummer et al., 1981b; Evans et al., 1993).

The portal vein receives blood from several abdominal organs, including the gastrointestinal tract, pancreas, and spleen. The major contributants of the portal vein are the gastroduodenal vein, splenic vein, and caudal and cranial mesenteric veins (Schummer et al., 1981b).

The microcirculation in the liver comprises all intrahepatic vessels smaller than 300μm in diameter. Thus, it includes portal venules, hepatic artetrioles, sinusoids, central venules, and lymphatics (McCuskey, 2008).

3.3.2. Kidneys

The kidneys are supplied by renal arteries branching directly from the abdominal aorta. Renal artery bifurcates into dorsal and ventral branches, each of which divides further into a number of interlobar arteries (2-7), before or after the renal hilus. At the corticomedullary junction, the interlobar arteries divide into numerous arcuate arteries, interlobular arteries, and afferent arterioles entering the glomerulus, glomerular arterioles, efferent arterioles leaving the glomerulus (at the level of the outer medulla) and entering the capillary network before draining back to the venous system (Figure 1) (Schummer et al., 1979; 1981a; Christensen et al., 1993).

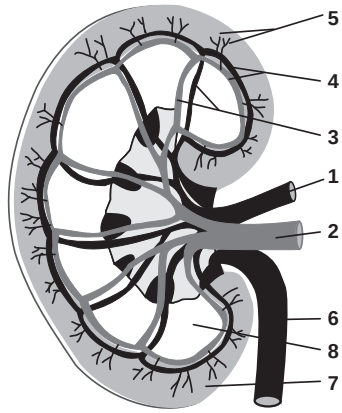

Figure 1 *The vasculature of the kidney: renal artery (1), renal vein (2), interlobar artery and vein (3), arcuate artery and vein (4), and interlobular artery and vein (5). Ureter (6), kidney cortex (7), and medulla (8).*

The microcirculation is divided in cortical, outer, and inner medullary systems. The difference in the perfusion between the kidney cortex and medulla is that the cortex is supplied by arterial blood, whereas the blood coming to the medulla (efferent arterioles) has already passed through the capillary system, in the glomerulus at the corticomedullary junction, or parts of it (Schummer et al., 1979; Pallone et al., 1998). There are shunting vessels directly to the medulla supplied by periglomerular pathways, but the extent of blood flowing through this system is unknown (Pallone et al., 2003).

3.3.3. Spleen

The spleen is supplied by the splenic artery, which arises from the celiac artery. The major draining vein is the splenic vein, which drains into the portal vein. The splenic artery branches into three to five branches; to the pancreatic, left gastroepiploic, splenic and short gastric arteries. The spleen has 25 smaller splenic arterial branches that pass through the hilus, terminating into the reticular meshwork (Schummer et al., 1981a).

The spleen is divided functionally into white and red pulp, and blood vessels (Schmidt et al., 1983) (Figure 2). In cats, the white pulp consists of mainly lymphatic nodules, whereas the major role of the red pulp is to store, concentrate, and filter erythrocytes, lymphocytes, and monocytes (Song et al., 1971). In cats, no direct arterio-venous connections have been found in the spleen, contrarily to dogs, and thus, the spleen of cats is said to be non-sinusoidal (Schmidt et al., 1982; 1983) (Figure 2). The blood flows from arteries to veins through the reticular meshwork of the red pulp. The pulp venules are non-anastomosing, and receive flow freely from the reticular meshwork via open ends and fenestrations (Levesque et al., 1976; Schmidt et al., 1983) (Figure 2). Furthermore, the flow of red blood cells in the spleen of cats has been demonstrated in kinetic studies (Song

et al., 1971; Levesque et al., 1976) to be divided into three compartments. Thus, a definitive picture of the circulatory pathways through the spleen of the cat is difficult to obtain because the microvascular bed is not formed from a system of closed vessels (Schmidt et al., 1983).

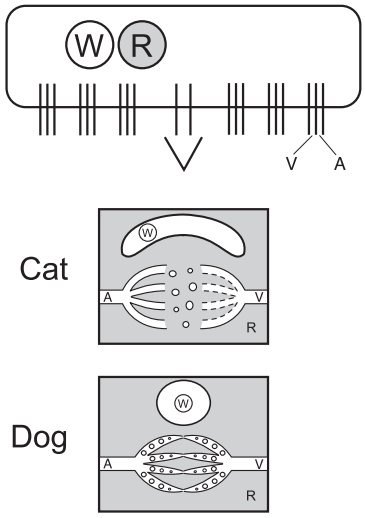

Figure 2 *Structure and vasculature of the spleen. The microvascular structure is in magnification: red pulp (R), white pulp (W) with, arteries (A), and veins (V).*

3.3.4. Pancreas

The pancreas is supplied by cranial and caudal pancreaticoduodenal, splenic, and gastroduodenal arteries, which arise from the celiac artery, with the exception of the caudal pancreaticoduodenal artery, which arises from the cranial mesenteric artery. The left part of the pancreas is supplied by branches from the splenic, cranial pancreaticoduodenal and gastroduodenal arteries, all arising from the celiac artery (Schummer et al., 1981a).

The vascular structure of the pancreas comprises a fine reticular network of vessels arranged in an intralobular vascular pattern. Within the interstitial spaces, larger interlobular vessels are evident. Microvascular segments of pancreatic perfusion are arranged in a densely meshed network of nutritive capillaries, afferent arterioles, and post-capillary venules (Geboes et al., 2001; Schaser et al., 2005).

Arterial arcades are formed between the major supply arteries, and numerous anastomoses are present within the substance of the pancreas. Within the pancreas, the arterial branches form an interlobular plexus in the connective tissue of the interlobular septa. From these plexuses, single intralobular arteries pass into each lobule, where they

form a fine reticular network supplying individual islets of Langerhans and then continue to adjacent acini. The veins in the pancreas correspond in general to the arterial pattern. They drain into the portal venous system behind the neck of the pancreas (Schiller et al., 1975; Geboes et al., 2001; Schaser et al., 2005).

3.3.5. Small intestine and mesenteric lymph nodes

The small intestine is mainly supplied by the cranial mesenteric artery and its branches. The duodenum is supplied by the cranial and caudal pancreaticoduodenal arteries, the jejunum by 12-15 jejunal arteries, and the ileum by accessory cecal and ileocolic arteries, and mesenteric ileal branches of jejunal arteries (Schummer et al. 1981a). The mesenteric lymph nodes are supplied by jejunal arteries (Schummer et al., 1981b).

The arteries in the mesenterium divide and anastomose several, forming arcades. The last of these forms a marginal artery along the small intestine. The marginal artery is defined as the artery closest to, and parallel with, the wall of the intestine (Geboes et al., 2001). From the marginal artery, blood reaches the intestine via short, straight branches or the vasa recta. The vasa recta penetrate the external muscle layers of the bowel wall to reach a profusely anastomotic submucosal arterial plexus, from which arterioles for the mucosa, submucosa, and muscular layers originate. The lymphoid tissue of the small intestine is supplied by the submucosal plexus through interfollicular arteries between the lymphoid follicles and through follicular arterioles originating from the interfollicular arteries. Venous drainage of each of the small intestinal capillary beds passes to the submucosal venous plexus, which anastomoses both longitudinally and circumferentially in the bowel wall. This plexus is drained by short veins, which penetrate the external muscle layers, chiefly along the mesenteric margin and then pass to branches of the superior mesenteric vein in the mesentery. The superior mesenteric vein receives venous drainage of the distal duodenum, jejunum, ileum, appendix, caecum, ascending and transverse colon, and the right gastro-epiploic vein draining the stomach, before joining the splenic vein to form the hepatic portal vein (Geboes et al., 2001).

The mesenteric lymph nodes, also called jejunal lymph nodes, consists of a varying number (2-5) of nodes, and are located in the root of the mesentery on both sides of the jejunal arteries and veins in the cat (Schummer et al., 1981b). These nodes drain lymph from the entire small intestine and the body of the pancreas and from the colon and rectum via caudal mesenteric lymph nodes (Schummer et al., 1981b).

3.4. Safety of CEUS

3.4.1. Safety of USCAs

The gas inside the microbubbles is biologically so inert and stable that it will not react with the molecules of the body even when the bubbles break. Instead the gas is eliminated

from the lungs by exhalation (Morel et al., 2000; FDA 2001; Greis, 2004; EMEA, 2005). The shell is either metabolized by the liver or used directly as a component in cell membranes (Morel et al., 2000; Greis, 2004). Eventhough there are certain risks and adverse effects related to CEUS (Dijkmans et al., 2005; van Camp et al., 2007), they are mostly considered to be not serious (Blomley et al., 2007).

Compared to other imaging modalities using contrast, USCAs are very safe to use, even in patients with liver or kidney failure and in trauma patients (Jäger et al., 2004; Leen et al., 2004; Correas et al., 2006). Side-effects are rare and when they do occur are mostly mild and transient (Miller et al., 2000; Morel et al., 2000; FDA, 2001; EMEA, 2005). Cardiac arrhythmia and premature ventricular contractions are possible with contrast-echocardiography when high MI is used and the heart is imaged at end-systole (Miller et al., 2000; FDA, 2001; Cosgrove, 2004; Jäger et al., 2004; Leen et al., 2004; EMEA, 2005). In experimental studies performed with rats using high MI (> 0.8), transient myocardial damage was seen as an elevation in troponin T, however, no histopathological evidence of cellular damage or inflammation was noted (Chen et al., 2002). In addition, the study design (USCA dose, MI, triggered imaging, transducer frequency, size of patient) exaggerated the extent of myocardial damage in CEUS; this level of damage would not be expected in clinical use (Chen et al., 2002). With USCAs, there is a mild and transient risk of embolus formation as a sequela of bubble aggregation (Miller et al., 2000; Cosgrove, 2004). This has little, if any, clinical significance unless the patient has congenital ventricular septal defect, which allows blood to circulate from left to right, therefore allowing the blood and possible emboli to reach brain circulation (Cosgrove, 2004). Ironically diagnosing these shunts was one of the original indications of cardiac CEUS (Drobac et al., 1983). The microbubbles used nowadays have a short terminal half-life (5-7 min) in the circulation (Morel et. al, 2000; FDA 2001). Therefore brain damage due to gas emboli from microbubbles is unlikely to occur. In addition, the relatively small dose of the microbubbles in the circulation and the properties of microbubbles diminish the risk of bubble aggregation into almost zero (Cosgrove, 2004; Jäger et al., 2004).

3.4.2. Adverse effects of CEUS

The adverse reactions reported with USCAs are mostly mild and, transient (FDA, 2001; Piscaglia et al., 2006; Blomley et al., 2007; EPAR, 2005), occurring less commonly than with the use of contrast agents (containing either iodine or gadolinium) in other imaging modalities such as CT and MRI (Katayama et al., 1990a; 1990b; Miller et al., 2000; Kirchin et al., 2001; Cochran et al., 2002; Jäger et al., 2004; Leen et al., 2004; Piscaglia et al., 2006). No fatal adverse events have been reported in the clinical trials conducted to obtain marketing authorization for USCAs (FDA, 2001; EMEA, 2005), or in their clinical use in humans (Piscaglia et al., 2006), dog (O'Brien et al., 2004a; Ohlerth et al., 2008; Ivancic et al., 2009) or cats (Rademacher et al., 2008; Kinns et al., 2010).

In medicine, the overall incidence of reported adverse effects of USCAs is less than 10% (FDA, 2001; EPAR, 2005). The most commonly (1-10 %) reported adverse effects (headache, altered sensation at injection site, nausea, flushing, paraesthesia, and taste perversion) have been mild in large clinical trials and have not required treatment

(Kitzman et al., 2000; Blomley et al., 2007; EMEA, 2005; EPAR, 2008; FDA, 2008). Moderate to severe adverse effects, requiring treatment, such as pain, nonspecific pain, pharyngitis, itching, rash, abnormal vision, dry mouth, dizziness, headache, hypotension, personality disorder, insomnia, respiratory disorders, nervousness, hyperglycemia, peripheral edema, eccymosis, and sensory-motor paresis, occur even less frequently (0,1-1 %) (FDA, 2001; EPAR, 2005; 2008; Piscaglia et al., 2006; Blomley et al., 2007). However, similar symptoms as listed above have been reported also after iv injections of saline (Nanda et al., 2002). The overall reported rate of adverse effects in a post-marketing study of Sonovue® contrast agent by Piscaglia et al. (2006) was 0,125% and 0,0086% for serious adverse effects requiring treatment. The reporting rate of serious adverse effects has been reported to be higher with cardiac imaging (0,019%) than with abdominal imaging (0,0078%) (Blomley et al., 2007).

The ultrasound itself has been proven to cause some thermal effects on tissues (Abramowicz et al., 2008; O'Brien et al., 2008). Adding USCA increases these thermal effects (Prosperetti et al., 1991) as a function of acoustic power, focal depth and USCA dose (Wu, 1998). This should be taken into account, when imaging sensitive tissues like the brain or eye with or without contrast agents. However the body system is well protected from oxidative injury caused by free radicals and cell damage produced by cavitation. In addition, similar capillary ruptures that could occur after CEUS happen in the body system daily even without CEUS or basic ultrasound, e.g. due to coughing in the lungs or walking in the soles of the feet.

3.4.3. Contraindications

The list of contraindications has undergone many changes in the last ten years. Both the European Medicines Agency (EMEA) and the US Food and Drug Administration (FDA) have changed their recommendations and list of contraindications for the use of USCAs in severely ill patients or cardiac patients. However, due to recent studies, both EMEA and FDA have later withdrawn some of the previously given contraindications of use (EMEA, 2005; FDA, 2008) because they determined that, in some patients, the benefits for the diagnostic information that could be obtained through the use of USCAs may outweigh the risk for serious cardiopulmonary reactions, even among some patients at particularly high risk for these reactions. The contraindications removed by the FDA include: worsening or clinically unstable congestive heart failure, acute myocardial infarction or acute coronary syndromes, serious ventricular arrhythmias or high risk of arrhythmias due to prolongation of the QT interval, respiratory failure, severe emphysema, and pulmonary emboli or other conditions that cause pulmonary hypertension (FDA, 2008).

The use of USCAs is in general contraindicated in patients with cardiac or pulmonary level right to left shunt, severe heart failure, recent acute coronary syndrome, unstable ischemic cardiac disease, pulmonary hypertension, uncontrolled hypertension or adult respiratory distress syndrome (Jäger et al., 2004; EMEA, 2005; Claudon et al. 2008). The cardiac contraindications listed above are opposed by many leading human cardiologists using CEUS (Blomley et al., 2007), since the true causal relationship with the previously occurring deaths in cardiac patients who had undergone contrast-enhanced-stress-echo

studies has, not been indisputably shown (Cosgrove, 2006; Main, 2009; Blomley et al., 2007). Furthermore, in a large post-marketing study, no increase in mortality risk has been associated with contrast-enhanced-echography in hospitalized patients (Kusnetzky et al., 2008).

No studies of the use of USCAs in pregnant or lactating animals or humans exist, and whether the gas component of USCA is excreted in milk is unknown (FDA, 2001; Cosgrove, 2004; Jäger et al., 2004; Claudon et al. 2008; EPAR, 2005). Animal studies have not indicated harmful effects with respect to pregnancy, embryonal or fetal development, parturition or postnatal development (EPAR, 2005). Furthermore, the microbubbles do not travel through the placenta in most species, due to the protective effects of the placenta and separate circulatory systems.

3.4.4. Suspected pathophysiology of cellular damage in kidneys caused by CEUS in laboratory animals

The potential of CEUS in causing kidney injury has been studied in rats, mice (Miller et al., 2007; 2008; 2009; Williams et al., 2007), and pigs (Jiménez et al., 2008; Miller et al., 2010). Mild and transient effects on vasculature, such as microvascular damage in the kidneys, muscles, intestine, mesentery, lung, and heart, have been reported in small laboratory rodents experimentally (Miller et al., 2000; Dalecki, 2007; Williams et al., 2007; Miller et al., 2008). The imaging settings in these studies have, however, been quite different from those used in clinical scanning (Miller et al., 2000; Williams et al., 2007; Miller et al., 2008; 2009; 2010). Previous studies have indicated renal cellular injury, due to glomerular capillary rupture and hemorrhage (Wible et al., 2002; Miller et al., 2007; ; Williams et al., 2007; Miller et al., 2008; 2009; 2010). Clinically, this was detected as hematuria 5 min to 24 h post-CEUS (Miller et al., 2007; Williams et al., 2007; Miller et al., 2008). Histological analysis in these earlier studies showed glomerular capillary rupture, and in the proximal tubules, phagocytosis of erythrocytes and degeneration of the resorptive epithelium, indicative of acute tubular necrosis (Wible et al., 2002; Miller et al., 2007; Williams et al., 2007; Miller et al., 2008; 2009; 2010). The effect was, however, transient, and significantly reduced by 24 h post-CEUS (Williams et al., 2007).

The capability of CEUS to induce cellular damage has been shown to be highly dependent on transducer frequency, MI, duration of exposure, and USCA type and dose (Miller et al., 2000; Wible et al., 2002; Miller et al., 2007; Williams et al., 2007; Miller et al., 2008), most of these parameters are different from those generally applied to clinical patients. In these experimental studies, glomerular hemorrhage was induced only with lower frequencies (1.5-3.2 MHz) combined with high ultrasound exposure (MI of 0.78 – 1.9, 1 to 9 min, intermittent imaging) and USCA infusion (Miller et al., 2008; 2009; 2010). On the other hand, no glomerular damage could be induced with the higher transducer frequencies (5.0-7.4 MHz), not even with the highest allowed exposure (MI of 1.9) in diagnostic ultrasound (Miller et al., 2008). The clinical significance of these effects is unclear in both human and veterinary medicine. Furthermore, no evidence of kidney damage was found in histological analysis in a recent study performed with pigs at a relatively high ultrasound exposure (transducer frequency 1.5 MHz, MI of 0.2 to 0.5,

Sonovue® infusion, continuous imaging) after CEUS (Jiménez et al., 2008). However, in another recent study performed with pigs using high ultrasound exposure (transducer frequency 1.5 MHz, MI of 1.2 to 1.9, Definity® infusion, intermittent imaging), glomerular capillary hemorrhage was observed (Miller et al., 2010). The differences between these two studies (Jiménez et al., 2008; Miller et al., 2010) are in ultrasound exposure (MI, scanning time), the USCA used, and imaging protocol (continuous vs. intermittent).

3.4.5. Detection of renal cellular injury

To detect an acute and transient kidney injury that might be potentially induced by CEUS, sensitive biomarkers are needed. Many urinary enzyme activities have been reported to increase earlier than blood urea nitrogen (BUN) or serum creatinine concentration, suggesting that they are sensitive early indicators of the risk of acute kidney injury in cats (Hardy et al., 1985; Jepson et al., 2009), dogs (Greco et al., 1985; Heiene et al., 1991; Rivers et al., 1996; Clemo, 1998; Coca et al., 2008) and human (D'Amico et al., 2003; Westhuyzen et al., 2003). Previous studies have documented the use of a variety of urinary activities, such as N-acetyl-β-D-glucosaminidase (NAG), gamma-glutamyl transferase (GGT), and alkaline phosphatase (ALP), in association with acute kidney injury (AKI) in various animal species, including cats (Hardy et al., 1985; Sato et al., 2002b; Jepson et al., 2009), dogs (Greco et al., 1985; Gossett et al., 1987; Heiene et al., 1991; Uechi et al., 1994a; Grauer et al., 1995; Rivers et al., 1996; Palacio et al., 1997; Sato et al., 2002a), sheep (Garry et al., 1990; Raekallio et al., 2010) and rats (Ogura et al., 1996).

Urinary enzyme activities have been investigated in feline patients with drug induced AKI (Hardy et al., 1985), with other types of urinary disease (Sato et al., 2002b; Jepson et al., 2009), and with hyperthyroidism (Lapointe et al., 2008). The circadian variation (Uechi et al., 1998) and changes in renal enzyme activities in the kidney with age have also been evaluated (Kaler et al., 1978). The changes in the enzyme activities caused by AKI or chronic kidney disease in cats (Hardy et al., 1985; Sato et al., 2002b; Lapointe et al., 2008; Jepson et al., 2009) have been similar to those seen in humans (Bazzi et al., 2002; Westhuyzen et al., 2003; Han et al., 2008) and dogs (Heiene et al., 1991; Uechi et al., 1994a; Rivers et al., 1996; Palacio et al., 1997; Clemo, 1998; Heiene et al., 2001; Sato et al., 2002a; Narita et al. 2005). However, in humans enzymuria has been reported to occur also as response to physiologic conditions or mild injury that does not precede AKI (D'Amico et al., 2003; Westhuyzen et al., 2003). NAG activities may also be increased in conditions without AKI (Iqbal et al., 1998; 2003; Kavukcu et al., 2002), for example in hypertension (Harmankaya et al., 2001), obesity, and diabetes (Corral et al., 1992; Fujita et al., 2002). Thus, when diagnosing active acute kidney cellular injury, it is important to detect persistently elevated and increasing urinary enzyme activities.

4. Aims of the study

The main objective of this thesis was to investigate the use of CEUS with varying ultrasound equipment, contrast-specific software, imaging protocols, and methods of measurements in cats. Detailed aims were as follows:

1. To develop an examination protocol for using abdominal CEUS and to evaluate the perfusion of normal abdominal organs (liver, kidney, spleen, small intestine, mesenteric lymph nodes, and pancreas) in healthy, anesthetized cats (I; IV).

2. To determine the effect of the size and placement of the ROI on perfusion parameters (II).

3. To study the effect of certain anesthetic agents on perfusion in the feline spleen with CEUS (IV).

4. To evaluate the safety of CEUS in feline kidneys (III).

5. Materials and methods

5.1. Test animals (cats)

The cats participating in our studies had earlier been used in other research projects assumed not to have an effect on the cats' health. The protocols were approved by the Institutional Animal Care and Use Committee at the College of Veterinary Medicine, Kansas State University, and the College of Veterinary Medicine, University of Illinois.

5.1.1. Group 1

Ten clinically healthy, young (5-6 months), intact male (mean 4.0 kg, range 3.6-4.3 kg) domestic short-hair cats were included in the studies (I; II; IV group 1). The cats were purpose-bred and group-housed. Clinical examinations were performed on each cat with complete blood count (Hb, Hct, RBC, WBC, Plt, MCV, MCH) and serum biochemistry (ALP, ALT, AST, bile acids, total bilirubin, GGT, BUN, creatinine, Na, K, Mg, Ca, P, total protein, albumin) to exclude metabolic disease. Urinalysis was also performed (specific gravity, protein, pH, sediment, culture) to exclude infections and hematuria. A 25-gauge intravenous catheter was placed in a cephalic vein during anesthesia. The indication for anesthesia was concurrent neutering for later adoption of the cats.

5.1.2. Group 2

Eight young to middle-aged (2-4 years), domestic short-hair cats were included in the studies (III; IV group 2). Five of the cats were neutered females, and three were neutered males. The mean bodyweight was 5.2 kg (range 4.2-6.3 kg). The cats were purpose-bred and group-housed. At the start of this experiment, the animals were clinically healthy and had no ongoing treatments. Clinical examinations were performed on each cat with complete blood count (Hb, Hct, RBC, WBC, Plt, MCV, MCH), serum biochemistry (ALP, ALT, AST, total bilirubin, GGT, BUN, creatinine, Na, K, Mg, Ca, P, total protein, albumin), and urinalysis to confirm the health of the cats both before and after the study. Two of the cats had mildly elevated BUN and creatinine concentrations before and after the study, but none of the cats became clinically ill. The cats had permanent jugular (6 cats) or saphenous (2 cats) catheters that had been placed 3-5 days before the study to facilitate collection of blood samples and injection of the USCA to avoid unnecessary pain and stress. These catheters had been placed under sedation with 0.05 mg/kg of butorphanol, 0.04 mg/kg of medetomidine and 0.009 mg/kg atropine given intramuscularly (im). The effect of medetomidine had been reversed with 0.04 mg/kg atipamezole given im.

5.2. Anesthesia of the cats

5.2.1. Group 1

Cats in group 1 were anesthetized for all of the imaging procedures (I; II; IV). They were pre-medicated with atropine (0.02 mg/kg sc), and sedated with acepromazine (0.06-0.1 mg/kg sc) and morphine (0.25-0.5 mg/kg sc). General anesthesia was induced with diazepam (0.3 mg/kg iv) and ketamine (6 mg/kg iv).

5.2.2. Group 2

Cats in group 2 (III; IV) were first imaged awake (2awake) and later anesthetized (2anesth). The left kidney and spleen (2awake) were imaged while the cats were awake. After 48 h, the spleen was again imaged, but this time the cats were anesthetized (2anesth) to investigate the effects of anesthesia on CEUS of the spleen. The cats were first sedated with butorphanol (0.2-0.4 mg/kg im) and anesthesia was induced 15 min later with one to three boluses (adjusted by individual response) of propofol (1-3 mg/kg iv), and maintained with one to two additional boluses, as necessary to maintain the anesthesia. Imaging was started 10 min after the induction of anesthesia. After all imaging was completed, the cats were monitored clinically for 4 h for any possible side-effects.

5.3. Ultrasound imaging

5.3.1. Machinery

Cats were imaged using linear transducers of 8-15 MHz (group 1) or 3-11 MHz (group 2), with transmit frequencies of approximately 7 MHz (group 1) or 2.95 MHz (group 2), on ultrasound machines with contrast-specific softwares (CPS [Cadence Contrast Pulse], Siemens Medical Solutions, and CnTI [Contrast Tuned Imaging], Biosound Esaote Inc.) available from Kansas State University, and University of Illinois, repectively. Both of these ultrasound systems are optimized for harmonic signal display and detection of nonlinear signals with either pulse sequencing (CPS) or subtraction (CnTI) techniques with low MI.

Table 1 *Machine settings for each imaged organ: liver, left (lt) kidney, spleen, pancreas, small intestine (SI), and mesenteric lymph nodes (Mes Lnn). No time gain compensation (TGC) was used.*

Organ	Cat group	MI	Power	Frequency	Frame rate	Depth	Focal zone	TGC
Liver	1	0.32	16dB	7MHz	16Hz	4.5cm	2cm & 3cm	no
Kidney lt	1	0.32	16dB	7MHz	16Hz	4.5cm	2cm & 3cm	no
Spleen	1	0.32	16dB	7MHz	16Hz	4cm	2cm & 3cm	no
Pancreas	1	0.33	16dB	7MHz	16-21Hz	3cm	1cm & 2cm	no
SI, Mes Lnn	1	0.31	16dB	7MHz	16-21Hz	3cm	1cm & 2cm	no
Spleen	2	0.04	5% / 50-55%	2,95MHz	18-26Hz	2.2-2.9cm	1.5cm	no
Kidney lt	2	0.04	5% / 50%	2,95MHz	18Hz	3.6cm	2.5cm	no

5.3.2. Transducer positioning

The hair was clipped over the ventrolateral abdomen (I; II; IV) or above the spleen and left kidney (III; IV). Alcohol and gel were applied to the skin and the transducers were manually positioned by the author during all imaging throughout the studies. Care was taken to keep the transducer in the same location in relation to the organ imaged and at approximately the same depth during the scanning; however, slight differences existed between the groups (1, 2) in the location and depth in the imaging of the spleen (IV). In group 1, images were collected from mid-body to the tail of the spleen. In group 2, images were collected from mid-body of the spleen, close to the branches of the splenic artery entering the hilus.

5.3.3. Imaging parameters

In group 1, the MI was maintained at a medium level (Table 1) depending on the depth of view. An intermediate MI was chosen for image optimization with the selected transmit frequency, machine system and contrast medium. Ultrasound scanning parameters, including depth, time gain compensation (TGC), overall gain, and focal zones, were standardized (Table 1). Two focal zones were placed at the level of or just below the organ imaged. The number and placement of focal zones were optimized for better image quality with the selected transducer frequency and imaging depth.

Organs were imaged in the following order: liver, spleen, left kidney, pancreas, small intestine, and mesenteric lymph nodes. The left kidney, left lobe of the liver and the pancreas were imaged separately in the sagittal plane. The small intestine and mesenteric lymph nodes were imaged simultaneously in the transverse plane. A digital imaging series of 30 s with a frame rate of 16-22 Hz, depending on the depth of the organ imaged, was recorded after each contrast injection. The total length of the imaging was 2 min in 6/10

cats. Originally, this was thought to be sufficient to reach outflow of the contrast from each organ. This was, however, not the case with the spleen and kidney medulla.

In group 2, a low MI was used (Table 1). Adjustable scanning parameters were including depth, gain, output power, number and location of focal zones in relation to the target organ, standardized (Table 1). A 90-s digital imaging series with frame rates of 16-25 Hz, depending on the depth and organ, was recorded for each contrast injection.

5.3.4. Contrast agent administration

Definity®-contrast medium was used in these studies. Definity® consists of octafluoropropane-gas-containing microbubbles encapsulated in a phospholipid shell. The contrast medium was prepared by shaking the vials with a mixing device according to the manufacturer's instructions. All cats received multiple (group 1: one to two, group 2: three to six) bolus injections (0.1 ml) of contrast medium iv (group 1: cephalic vein, group 2: jugular or saphenous vein) followed by a bolus of 0.5 ml of heparin-saline. The injections were given in a standardized manner by the same person in each study. The time between the injections (from the end of injection to the beginning of the next) was approximately 2 min (group 1) and/or until no contrast was visible (group 1: 2 min, group 2: 1-2 min). Between the injections an attempt was made to destroy the bubbles by continuous scanning of the imaged organ and cranial abdomen and aorta with fundamental ultrasound and output power adjusted to 100-80%, until background echogenicity was similar to pre-injection levels, until no contrast was visible. In group 2, one of the cats had to be imaged on an additional day, due to poor image quality and non-co-operative behavior.

5.4. Image analyses

5.4.1. Quantitative analyses of the perfusion in the liver, spleen, kidneys, pancreas, small intestine and mesenteric lymph nodes (I; IV group 1)

Standardized TICs were created on line from the raw imaging data (ACQ) in selected ROIs for each organ, representing the signal intensity (dB) in relation to time (s) (I; II). The data were then exported and evaluated with an external computer using commercial software (Excel and Prism) to obtain functional perfusion parameters. Care was taken not to include any adjacent tissues (mesentery, falciform fat) or larger vessels inside the ROI. In the pancreas, small intestine, and mesenteric lymph nodes, the size of the ROI was chosen so that it covered the organ parenchyma as well as possible. However, the ROI was limited in size when avoiding large vessels near the organ of interest. Artifactual data, such as data from adjacent tissues introduced within the ROI during respiratory motion, were removed. The placement of the ROI is illustrated in Figure 4 (yellow). In the liver, the placement of the ROI was left from midline, but the placement varied slightly between individuals due to respiratory motion and image quality. The functional perfusion

parameters chosen for analysis were according to Du et al., (2008) and Waller et al., (2007) as follows:

- Arrival time (AT, [s]), defined as the time point when contrast level rises above baseline in the TIC, followed by a further rise (10% above baseline).
- Time to peak intensity (TTP_{inj}, [s]), measured from the end of the injection, defined as the time when intensity peaks following AT.
- Baseline intensity (BI, [dB]), defined as the signal intensity at AT.
- Peak intensity (PI, [dB]), defined as maximal signal intensity at TTP_{inj}.
- Time to peak intensity from the initial rise (TTP_{inr}=TTP_{inj}-AT, [s]).
- Wash-in rate (Wi, [dB/s]) was calculated from the data subset between 10% above baseline to 90% of the peak intensity. This avoided the use of toe and shoulder in the time intensity curve. The data were tested for linearity by assessment of significance ($p<0.05$) and R-square (> 0.7) to validate the use of linear regression analysis.
- Wash-out rate (Wo, [dB/s]) was calculated from the data subset between 90% below the peak intensity, where all subsequent points continued to decline, until 20% above the previous baseline value or until the final point measured (liver, spleen, renal medulla). The data were then regressed for linearity.

A detailed illustration of the perfusion parameters is presented in Figure 3.

The liver, kidney cortex, and medulla were imaged in all ten cats. In addition the pancreas, small intestine, and mesenteric lymph nodes were imaged in eight cats (8/10). Wash-out was calculated in 9/10 cats in the kidney medulla due to a very gradual sloping within the 30-s time interval. In one cat, the wash-out of the kidney medulla was gradual and was not measured within the first 30-s. Wash-out in the pancreas was calculated in 7/10 cats due to poor image quality in one cat. In 8/10 cats, data for the liver and kidney cortex were obtained by averaging two injections. In the other two cats, the second recording and corresponding TIC was rejected because of poor image quality. In kidney medulla (10/10), pancreas (8/10), small intestine (8/10) and mesenteric lymph nodes (8/10), the data were obtained from one injection.

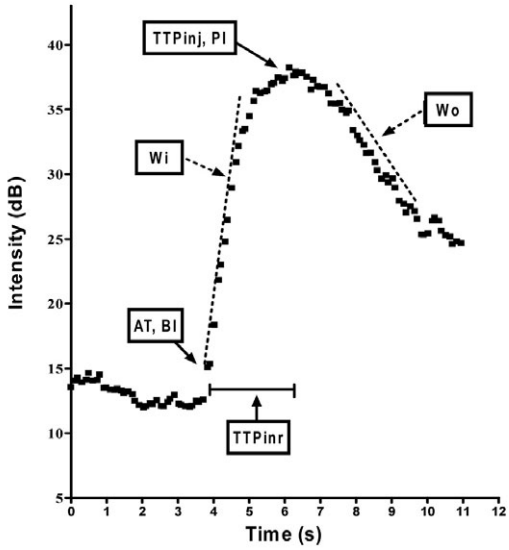

Figure 3 *Time-intensity curve (TIC) example from kidney cortex. For more details, see the text.*

5.4.2. Different methods of measuring or estimating perfusion

The perfusion measurements estimated using three slightly different methods were compared by the same trained person: 1) ultrasound video combined with TIC, 2) numerical data from the TIC, and 3) visual estimation from the ultrasound video. The perfusion parameters (AT, TTP_{inj}, BI, PI) obtained with different methods, were compared with each other statistically. In the visual estimation from the video, only timing parameters (AT, TTP_{inj}) could be estimated and compared with other methods. The comparisons were made in data obtained from the kidney cortex (cat group 1). These data have not been previously published.

5.4.3. Effect of ROI size and location on measurements of perfusion in CEUS (II)

Standardized TICs were drawn from selected ROIs in the cortex of each kidney. The data were manually edited by simultaneously analyzing the ultrasound images and TICs frame by frame to remove any false peaks and troughs from the TIC of due to respiratory motion. The functional perfusion parameters were chosen according to previous reports (Du et al., 2008; Waller et al., 2008) as follows: AT, [s]; TTP_{inj}, [s]); BI, [dB]; PI, [dB]; TTP_{inr}=TTP_{inj}-AT, [s]; Wi, [dB/s]; and Wo, [dB/s].

To study the effect of the location of the ROI on obtained values, three similar-sized (oval, length 0.5 cm) ROIs were placed in a row on the near field cortex at approximately the same depth (1-1.5 cm, Figure 5. ROI 1). The amount of subcutaneous and abdominal fat between the kidney and the body wall varied, causing small differences in the depths.

To examine the effect of ROI placement on depth direction (ROI 2), three additional ROIs were placed in a column (at depth 1 cm, 1.5-2 cm, and 2-2.5 cm) on the cranial cortex of the left kidney (Figure 4). Due to the round shape of the cat kidney, these ROIs could not always be placed exactly in a straight vertical line. To investigate the effect of size, three differently sized ROIs of length of approximately 0.3 cm, 0.6 cm, and 1.2 cm were placed in a row at the same depth in the near field cortex of the left kidney. The depth of the ROI's in the size correlation was matched with the depth of the horizontal placement comparison (ROI 1).

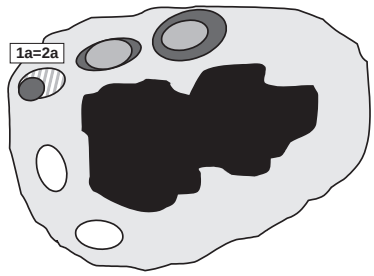

Figure 4 *Placement of the ROIs 1 (grey), 2 (white) and 3(dark grey) in the kidney cortex. The same ROI 1a (= 2a) was used in ROIs 1 and 2.*

5.4.4. Estimation of perfusion patterns in the spleen (IV)

The timing and grade of both heterogeneity and homogeneity of the spleen were estimated in a standardized manner by the same trained person in all groups (1, 2awake, 2anesth). This grading was developed to estimate the perfusion patterns visually due to differences in the machinery and therefore in the quantitative analysis of the perfusion between the groups. The person estimating the timing and grade was blinded from the identifier information on the ultrasound clips, and the clips were presented in randomized order. The grade (1-4) of heterogeneity was estimated at the time when the spleen was most heterogeneous as follows (Figure 5): grade 1, slightly mottled, less-enhanced areas not well defined; grade 2, moderately heterogeneous, regional, small (diameter < 0.5 cm) non-enhanced areas; grade 3, heterogeneous, regional, medium-sized (0.5 < diameter ≤1.0 cm) non-enhanced areas; grade 4, strongly heterogeneous, regional, large (diameter > 1 cm) non-enhanced areas. The grade of homogeneity (1-3) was estimated when the spleen was the most homogeneous as follows (Figure 6): grade 1, entirely homogeneous; grade 2, almost homogeneous; grade 3, obviously mottled, not homogeneous

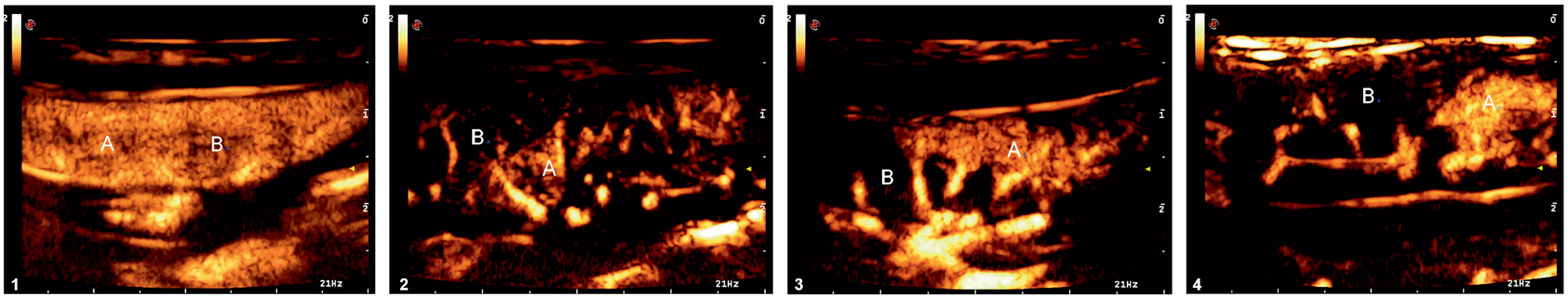

Figure 5 *Ultrasound images of different heterogeneity grades (1-4) of the spleen (n=8). The grade (1-4) of heterogeneity was estimated at the time point, when the spleen was the most heterogeneous (≈ 5 s). For more details, see the text.*

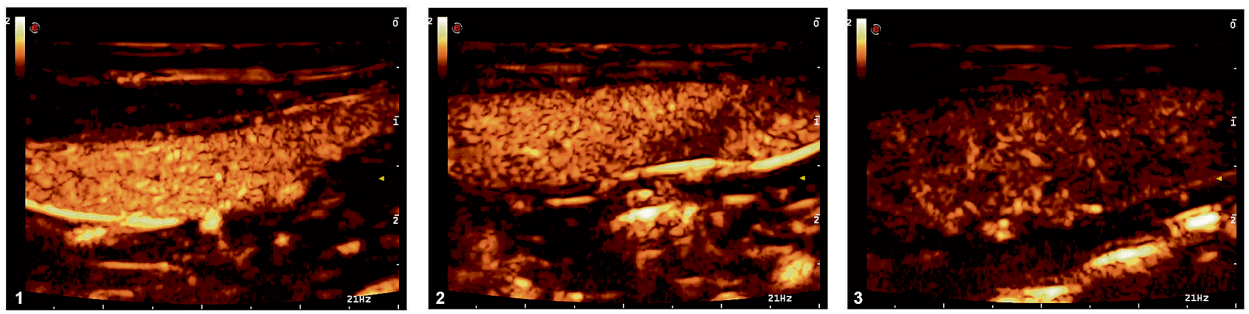

Figure 6 *Ultrasound images of different homogeneity grades (1-3) of the spleen (n=8). The grade of homogeneity was estimated at the time point, when the spleen was the most homogeneous (≥ 30 s). For more details, see the text.*

5.5. Sample collection and laboratory analyses (III)

Blood samples were collected from jugular or saphenous catheters already placed for another research protocol. Blood was collected before and 48 h after contrast ultrasound. Urine samples were collected by cystocentesis before and 4 h and 48 h after contrast ultrasound. Ultrasound guidance was used, when the bladder was small or difficult to palpate. The baseline samples (urine and blood) were taken 5 days before beginning the study to allow the bladder to recover from possible bleeding post-cystocentesis.

Urine composition (specific gravity, pH, protein, creatinine, sediment to detect hematuria) and urine enzymatic activities (ALP, GGT, NAG) were analyzed. To correct for variations in urine flow, the enzyme activities (U/l) were normalized for urinary creatinine concentrations (g/l) and given as a ratio (U/g). RBC counts from the sediment were classified for statistical analysis into four separate classes: Class 0, no red blood cells visible (0 RBCs/hpf); class 1, 1 to 10 RBCs/hpf; class 2, 10 to 100 RBCs/hpf; and class 3, more than 100 RBCs/hpf.

The blood samples and urine were kept in a refrigerator until centrifuged (3300 rpm, 5 min) at 4°C to remove cellular components and debris. All of the samples were processed within 4 h of collection. Serum biochemistry measurements were performed with a clinical chemistry analyzer (Roche Hitachi 917 analyzer 37°C, Roche Diagnostics GmbH). Urine was first analyzed with a dipstick (Chemstrip, Roche Diagnostics GmbH), and urine specific gravity was determined by refractometry. Urine protein was determined with benzethonium chloride reaction and creatinine with alkaline picrate method (Roche Hitachi 917 analyzer 37°C, Roche Diagnostics GmbH, calibrated for urine). The urine was then centrifuged and the sediment underwent microscopic examination. Urine enzymatic activities were analyzed with a clinical chemistry analyzer (Roche Hitachi 917 analyzer 37°C, Roche Diagnostics GmbH). The rest of the urine samples were frozen at -80°C to await further urine NAG assays. NAG activity was measured with a commercial kit (NAG-kit, Roche) using a colorimetric method one month after the urine collection.

5.6. Statistical analyses

Statistical analyses were conducted with statistical software (SPSS and Statistix) by the author with statistician consultation. Data calculated for each perfusion parameter included mean values and standard deviation. Bonferroni's correction was used for the obtained p-values. Statistical siginificance was set at $p<0.05$.

Analysis of variance with repeated measurements was used to compare the following:

1. The perfusion parameters of each organ (liver, spleen, left kidney, pancreas, small intestine, mesenteric lymph nodes) between cats (I).
2. The perfusion parameters between organs or organ groups (sub-group of small intestine, mesenteric lymph nodes, and pancreas) within cats (I).

3. The effect of the location and size of the ROI with the functional perfusion parameters (AT, TTPinj, BI, PI, Wi) on the kidney cortex (II).

Student's t-test with two-tailed p-value was used to analyze or compare the following:
1. The variance within and between cats in the liver and renal cortex (I).
2. The perfusion parameters between organs (pairwise testing) (I).
    a. Liver and kidney cortex
    b. Pancreas and small intestine
    c. Kidney cortex and liver, pancreas, small intestine
    d. Small intestine and pancreas, mesenteric lymph nodes
3. The perfusion parameters between the differently perfused splenic areas (group 1) (IV).
4. The time to the first appearance of the contrast in the spleen (AT_v) and the time to the spleen becoming heterogeneous ($TTHe_{inj}$) or homogeneous ($TTHo_{inj}$), each parameter assessed visually between groups 1 and 2anesth, and within cats in group 2 with (2anesth) and without (2awake) anesthesia.

Student's one-sample t-test was used to evaluate the difference between two different injections (repeatability) in the liver and kidney cortex data (I).

Pearson's correlation test was used to evaluate similar tendencies in the perfusion parameters between separate organs within the same cat (I).

Coefficient variation was used to estimate the amount of internal variation in the perfusion parameters (I).

Analysis of variance with randomized complete block was used to separate the effect of the depth and the size of the ROI from the variance between the cats and from the statistical noise in the PI (II).

Homogeneity of variance was tested from the PI in the depth and size comparison using Levene's test, O'Brien's test, and the Brown and Forsythe test (II).

Friedman's test (non-parametric) was used to compare
1. The perfusion parameters between the different methods (video and TIC, TIC only, visual estimation from the video only).
2. The urinary measurements taken before and 4 h and 48 h after CEUS (III).

Wilcoxon's Signed Rank test (non-parametric) was used to compare
1. Pairwise post hoc testing of perfusion parameters between the different methods (video and TIC, TIC only, visual estimation from the video only).
2. Pairwise post hoc testing of urinary measurements to determine the direction of the change (III).

3. Pairwise testing of blood measurements taken before and 48h after contrast ultrasound (III).

Fischer's exact test (non-parametric) was used to compare the grades of heterogeneity and homogeneity of the spleen both between groups 1 and 2anesth and within the cats in group 2 with (2anesth) and without (2awake) anesthesia (IV).

6. Results

6.1. Normal organ perfusion (I)

The qualitative, visual assessment of the perfusion patterns in each imaged organ was evaluated from the ultrasound video clips. The quantitative assessment of the perfusion parameters was measured as signal intensity vs. time from selected ROIs acquired from the generated TICs (Table 2).

6.1.1. Perfusion in the liver, spleen, kidneys, pancreas, small intestine and mesenteric lymph nodes (I; IV group 1)

The enhancement of the different organs varied in time and pattern (Figure 7). Achieving contact between the linear transducer and the cat was somewhat difficult and required a moderate amount of pressure, especially when imaging the liver. The image quality was therefore not always optimal for the entire liver. In general, the image was considered more heterogeneous in the liver than in the other organs (Figure 7b), with the exception of the kidney medulla and the less perfused areas of the spleen. After injection of the contrast agent, there was an immediate marked enhancement of the hepatic arteries and portal veins. This was followed by a more gradual enhancement of the liver parenchyma.

Enhancement of the spleen was very heterogeneous at the beginning of imaging (Figures 5 and 7c, Table 2). In most of the cats, the splenic parenchyma was enhanced in two or three phases (Figures 5 and 7c, Table 2): The large splenic vessels enhanced rapidly and intensely. This was followed by enhancement of the parenchyma surrounding these vessels (Figure 5, area A; Figure 7c, black ROI), followed by a more gradual enhancement of the remainder of the spleen (Figure 5, area B; Figure 7c, white ROI). Enhancement of the two differently enhanced splenic areas (A and B) reached equivalent intensity at approximately 20-25 s (Figure 7c, TIC). At this same time, the early enhanced areas (A) were already in wash-out phase (Figure 7c, TIC).

The kidney parenchyma enhanced in two phases (Figure 7a, Table 2): The contrast arrived first in the cortex (Figure 7a, black ROI), followed by a more gradual and sparsely spotted enhancement of the medulla (Figure 7a, white ROI). The enhancement of the cortex and medulla reached almost equal intensity at 30 s; by this time, the cortex was already in wash-out phase (Figure 7a, TIC).

The pancreas, small intestine, and mesenteric lymph nodes all enhanced early and very intensely immediately after the large supplying vessels (Figures 7d and 7e). Keeping the ROI in the middle of the scanned area, thereby avoiding larger vessels and adjacent tissues was more difficult in the liver and pancreas, the organs most affected by respiratory motion.

Table 2 *The perfusion parameters (mean ±SD). The statistical comparisons were made between 1) the kidney cortex and medulla, 2) two differently perfused splenic areas A and B, 3) the subgroup of the small intestine, pancreas and mesenteric lymph nodes, 4) the liver and kidney cortex, and 5) the liver and the subgroup of small intestine, pancreas, and mesenteric lymph nodes. Significant differences ($p<0.05$) in the perfusion parameters between organs or organ subgroups are indicated as letters (A= liver; B=kidney cortex; C=kidney medulla; D=small intestine; E=pancreas; F=spleen A; G=spleen B).*

Organ	**AT** (s)	**TTP_{inj}** (s)	**PI** (dB)	**Wi** (dB/s)	**Wo** (dB/s)
Liver	5.81 (1.96)^{B,D,E}	9.66 (2.9)^{B,D,E}	29.7 (3.15)^{B,D}	5.89 (3.38) ^{B,D,E}	0.23 (0.08) ^{B,D,E}
Spleen A	3.9 (1.22)	7.77 (1.4) ^{G}	32.5 (4.41) ^{G}	6.95 (2.8) ^{G}	0.52 (0.12)
Spleen B	4.02 (1.45)	25.1 (2.24) ^{F}	25.9 (5.42) ^{F}	0.81 (0.25)^{F}	-
Kidney cortex	3.96 (0.52) ^{A,C,D}	5.99 (0.61) ^{A,C,D}	32.4 (4.96) ^{C}	12.2 (2.38) ^{A,C}	3.12 (0.76) ^{A,C,D}
Kidney medulla	8.08 (2.76) ^{B}	21.8 (11.1) ^{B}	16.0 (5.75) ^{B}	1.48 (2.04) ^{B}	0.13 (0.06) ^{B}
Pancreas	4.1 (0.47) ^{A}	5.96 (0.85) ^{A}	23.8 (4.96) ^{A}	11.43 (4.92) ^{A}	4.03 (2.1) ^{A}
Small intestine	4.38 (0.46) ^{A}	6.47 (2.44) ^{A}	27.6 (5.02)	10.83 (2.96) ^{A}	3.08 (1.21) ^{A}
Lymph node	4.2 (0.61) ^{A}	6.37 (0.74) ^{A}	23.6 (4.37)	9.3 (2.45) ^{A}	2.79 (0.86) ^{A}

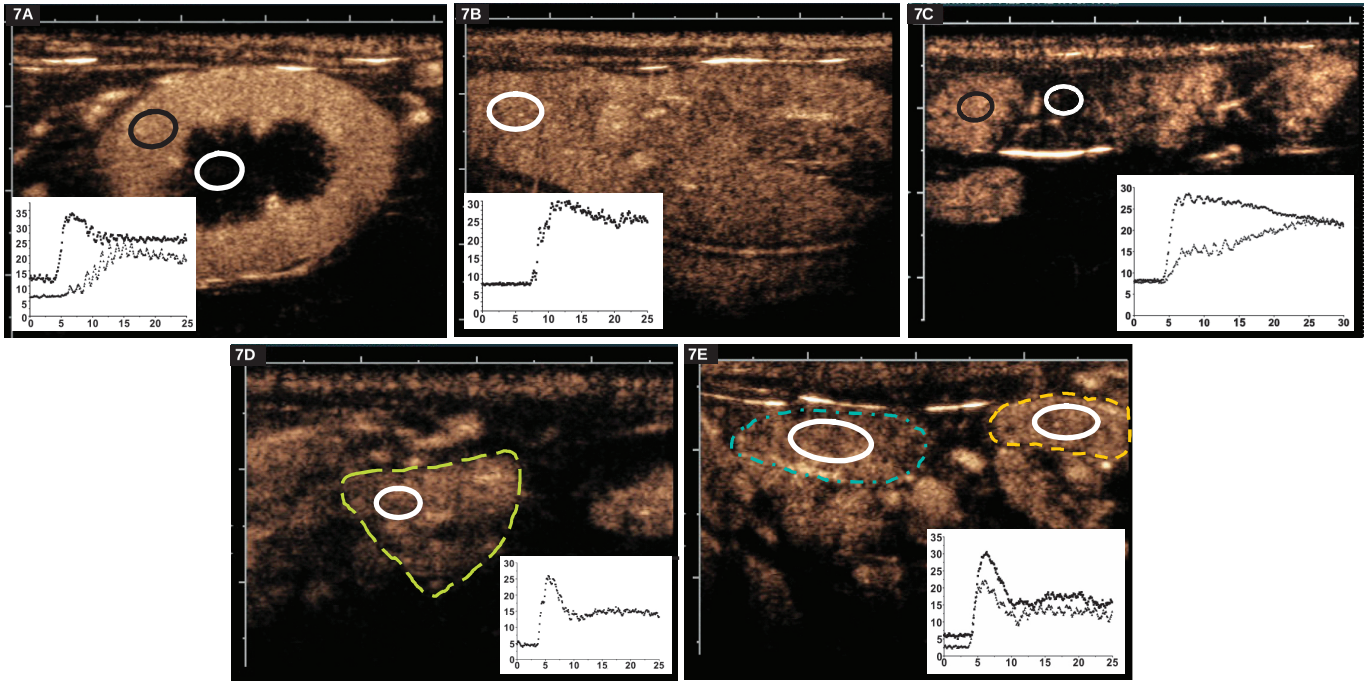

Figure 7 *The time of maximal enhancement in the kidney (A), liver (B), spleen (C), pancreas (D), small intestine, and mesenteric lymph nodes (E) of a healthy cat. Regions of interest (ROI) are encircled by solid black or white lines. In the kidney (7A), the black ROI represents the enhancement of the cortex and the white ROI the enhancement of the medulla. In the spleen (7C), the black ROI represents the enhancement of the early perfused areas, and the white ROI the late perfused areas. In part D, the outline of the pancreas is indicated by a dashed line (green). In part E, the small intestine and lymph node are encircled by dashed lines (yellow; small intestine, blue; mesenteric lymph node). Inset graphs provide corresponding time intensity curves (x-axis = time (s), y-axis = intensity (dB) from the ROIs). For more details, see the text.*

6.1.2. Differences in the perfusion between organs

The results of the statistical analyses from the comparison of perfusion parameters between organs are presented in Table 2. The differences between the kidney cortex and medulla were statistically significant in all perfusion parameters. This was considered to be unrelated to the small difference in the depth of the ROI between the cortex and medulla. This was further supported by visual assessment; the large difference in the enhancement between the cortex and medulla was considered to be more obvious than the mild attenuation of the signal intensity at the distal kidney cortex. The differences between the differently perfused splenic areas A and B were significant in all perfusion parameters, except AT. In the sub-group of the small intestine, lymph nodes, and pancreas, no significant differences were observed. The liver differed from the kidney cortex and pancreas in all of the perfusion parameters. Between the liver and small intestine, a significant difference arose in all parameters, except BI and PI. Moreover, a significant correlation emerged between the small intestine and lymph nodes in AT (r=0.943), BI (r=0.734), and TTP_{inj} (r=0.856), and between the kidney cortex and, small intestine in AT (r=0.822) and TTP_{inj} (r=0.938).

6.1.3. Repeatability

The intra-individual variation between the two separate injections (in the liver and kidney cortex data) was smaller than the interindividual variation. The numerical data from separate injections are presented in Table 3. In the liver data, however, a significant difference appeared in the BI between the injections (p=0.014).

Table 3 *Perfusion parameters from separate injections in the kidney cortex and liver presented as mean (±SD). The asterisk (*) indicates a significant difference between parameters.*

	AT (1.)	BI (1.)	TTP_{inj} (1.)	PI (1.)	TTP_{inr} (1.)
Kidney cortex	4.01 (0.50)	10.60 (2.56)	6.01 (0.81)	32.39 (5.95)	2.00 (0.69)
Liver	5.63 (2.50)	9.03 (3.26)*	9.72 (3.46)	29.51 (3.36)	4.08 (1.95)
	AT (2.)	**BI (2.)**	**TTP_{inj} (2.)**	**PI (2.)**	**TTP_{inr} (2.)**
Kidney cortex	4.01 (0.64)	10.70 (3.42)	6.04 (0.62)	32.25 (4.72)	2.03 (0.41)
Liver	6.56 (2.56)	11.22 (3.56)*	10.00 (3.34)	28.57 (3.60)	3.44 (1.00)

6.1.4. Comparison of different methods in measuring or estimating perfusion

A significant difference emerged in AT between the different methods (p=0.012) in the kidney cortex data (Table 4), when comparing the visual estimation with the combination of visual estimation from the video and TIC (p=0.048). However, the detected difference

was smaller than the difference in the accuracy between the methods (visual estimation only 1 s, other methods 0.01 s). The differences in AT and PI between TIC analysis and the combination of visual estimation of video and TIC reached statistical significance (p=0.063 and p=0.055, respectively).

Table 4 *Perfusion parameters presented as mean (±SD) from the method comparison in the kidney cortex data. The asterisk (*) indicates a significant difference between parameters.*

Method	**AT** (s)	**BI** (dB)	**TTP_{inj}** (s)	**PI** (dB)
TIC	4.01 (0.48)	10.60 (2.56)	6.01 (0.81)	32.39 (5.95)
TIC+Video	3.76 (0.65)*	10.39 (2.59)	6.60 (0.55)	33.30 (5.45)
Video	4.25 (0.46)*		6.69 (0.80)	

6.2. Importance of location and size of ROI (II)

Subjectively, the image quality appeared optimized and uniform in the near-field kidney cortex. Attenuation was observed by visual estimation in the far-field cortex. A significant difference was found in the peak intensity of the ROIs for both depth (Figure 8; p=0.027) and size (Figure 9; p=0.026). The mean PI decreased with increasing depth and increasing size of the ROI. The variance in PI was homogeneous between ROIs of varying depth and size (p>0.22 and p>0.46 respectively). However, there was no significant difference in the PI between the ROIs placed in a row in the near-field cortex (p=0.861) (Table 5).

Table 5 *Mean (±SD) of perfusion parameters (AT=arrival time, BI=baseline intensity, TTP_{inj} =time to peak intensity, PI =peak intensity, Wi=wash-in rate) as a function of regions of interest (ROIs) location, depth and size. ROI 1a,b,c were located in the near-field cortex at the same depth in equal sizes. ROI 2a,b,c were located in the cranial cortex at different depths, but equal in size. ROI 3a,b,c were located in the near-field cortex at the same depth, but in different (increasing) sizes. Differences in the mean PI were significantly different between both the ROIs at different depths and sizes ROIs.*

	AT (s) mean (SD)	BI mean (SD)	TTPinj (s) mean (SD)	PI (dB) mean (SD)	Wi (dB/s) mean (SD)
ROI 1a	4.09 (0.54)	10.21 (3.30) [A]	6.71 (0.73)	32.99 (4.08)	8.96 (2.30)
ROI 1b	4.17 (0.56)	12.56 (4.87) [A]	6.60 (0.71)	33.32 (6.50)	8.79 (2.47)
ROI 1c	4.17 (0.54)	12.26 (4.21) [A]	6.59 (0.52)	32.86 (7.65)	8.60 (2.36)
ROI 2a	4.09 (0.54)	10.21 (3.30)	6.71 (0.73)	32.99 (4.08) [B]	8.96 (2.30)
ROI 2b	4.29 (0.65)	9.34 (2.76)	6.79 (0.98)	29.86 (2.63) [B]	8.57 (2.26)
ROI 2c	4.11 (0.56)	9.25 (3.41)	6.72 (0.93)	27.71 (5.47) [B]	7.31 (1.73)
ROI 3a	4.13 (0.35)	11.97 (3.82)	6.58 (0.72)	34.52 (4.89) [C]	9.59 (2.56)
ROI 3b	4.11 (0.52)	11.44 (3.70)	6.60 (0.83)	33.18 (6.08) [C]	8.90 (2.32)
ROI 3c	4.12 (0.47)	11.41 (4.05)	6.56 (0.58)	31.43 (6.66) [C]	8.20 (1.91)

Significant difference between

A = ROI 1a, 1b, 1c (BI)

B = ROI 2a, 2b, 2c (PI)

C = ROI 3a, 3b, 3c (PI)

A significant difference was present in BI (p=0.006) at the time of the first contrast agent appearance with varying placement of the ROIs in a row in the near field cortex (Table 5).

No significant difference emerged within the set of ROIs 1-3 in the following parameters: AT, PI, and Wi (Table 5).

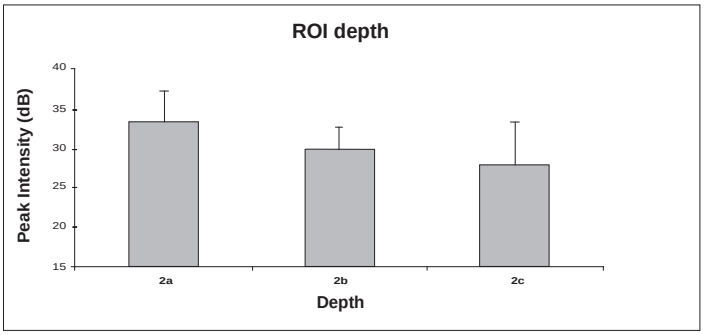

Figure 8 *Mean (±SD) of peak intensity (PI) as a function of ROI depth. Differences in the mean PI were significant between the ROIs at different depths.*

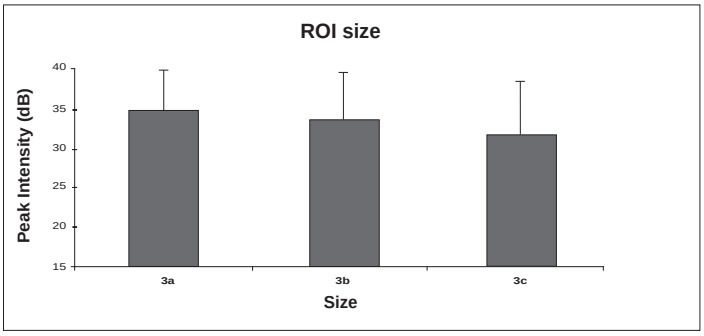

Figure 9 *Mean (±SD) of peak intensity (PI) as a function of ROI size. Differences in the mean PI were significant between the differently sized ROIs.*

6.3. Effect of anesthesia on splenic perfusion (IV)

The numerical results describing the perfusion of the spleen in group 1 are displayed in Tables 2 and 6. The results of the statistical analyses from the comparison of the awake and anesthetized cats are presented in Table 7. The differences between the differently perfused splenic areas A and B in group 1 were statistically significant in all perfusion parameters, except AT (Table 6). The time to first appearance of contrast medium (AT visual) in the spleen was significantly different between awake and anesthetized cats (2awake and 2anesth) (p=0.0307), but not between cats with different anesthesia protocols (groups 1 and 2anesth) (Table 7). The frequencies of the heterogeneous and homogeneous grades in the groups are presented in Figures 10 and 11. The least homogeneous grade 3, and the most heterogeneous grade 4 are overrepresented in group 2anesth (Figures 10 and 11). This indicates a difference in both the homogeneity and heterogeneity of the spleen between the groups, however, no significant difference was found between the groups in the heterogeneity or homogeneity grades.

Table 6 *Perfusion parameters calculated from the time-intensity curves (TICs) for the cat spleen in group I, with differently perfused splenic areas A and B are presented as mean (±SD). Significant differences (*p*<0.05) in perfusion parameters between the different areas (A and B) are indicated with an asterisk (*).*

	AT (s)	**TTPinj** (s)	**BI** (dB)	**PI** (dB)	**Wi** (dB/s)	**Wo** (dB/s)
Spleen A	3.90 (1.22)	7.77 (1.40) *	9.87 (2.07)	32.50 (4.41) *	6.95 (2.80) *	- 0.52 (0.12)
Spleen B	4.02 (1.45)	25.10 (2.24) *	9.26 (2.00)	25.90 (5.42) *	0.81 (0.25) *	

Table 7 *Numerical results estimated visually in all groups (1, n=10, 2, n=8) are presented as mean (±SD). The first contrast arrival (AT_v), the time to heterogeneity after the injection ($TTHe_{inj}$), and the time to the spleen becoming the most homogeneous after injection ($TTHo_{inj}$) are shown. Significant differences (*p*<0.05) in parameters between cat groups are indicated with an asterisk (*).*

Parameter	AT v (s)	TTHe inj (s)	TTHo inj (s)	Anesthesia
Group 1	4.20 (0.63)	5.20 (0.79)	28.30 (2.87)	Yes
Group 2awake	3.88 (0.64) *	4.63 (1.06)	30.75 (8.07)	No
Group 2anesth	4.75 (1.04) *	5.50 (0.93)	31.63 (5.01)	Yes

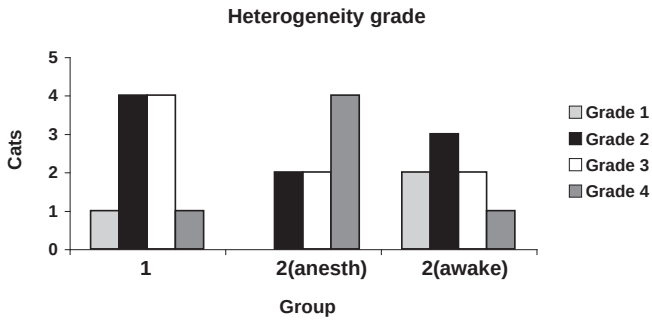

Figure 10 *Heterogeneity grades of the spleen between groups. The grade of heterogeneity was estimated visually when the spleen was the most heterogeneous (≈ 5 s). The cats were anesthetized in group 1(n=10) and group 2anesth (n=8), and awake in group 2awake (n=8).*

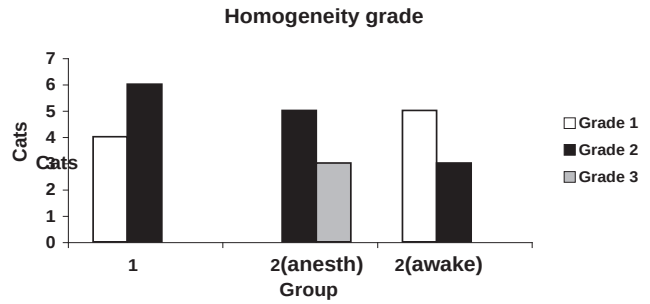

Figure 11 *Homogeneity grades between groups. The grade of homogeneity was estimated visually when the spleen was the most homogeneous (≈ 30 s). The cats were anesthetized in group 1(*n*=10) and group 2anesth (*n*=8), and awake in group 2awake (n=8).*

6.4. Effect of CEUS on kidneys (III)

The results of the laboratory values (urinalysis and biochemistry profile) are presented in Tables 8 and 9. There was a statistically significant increase in urine NAG (p=0.006) ratios when compared before and 48 h after contrast ultrasound (p=0.012), but not between before and 4 h after CEUS (p=0.123) (Table 8). No significant changes occurred in the mean GGT or ALP ratio, urine protein-creatinine ratio, pH, specific gravity, or urine red blood cell counts. A significant decrease in BUN concentration (p=0.024) (Table 9). No significant changes occurred in the rest of the analyzed blood constituents. Two of the cats had mildly elevated BUN and creatinine concentrations before and after the study, but none of the cats became clinically ill. One of the cats was later euthanized due to intestinal lymphoma and the rest of the cats were clinically healthy one year later.

Table 8 *Results of urinalysis of the eight cats presented as mean (±SD). Significant differences between the parameters are indicated with an asterisk (*, p<0.05). Urinary measurements were compared 3-5 days before (baseline), 4 h and 48 h after CEUS. RBC counts from sediment were classified as follows: Class 0=0 RBCs/hpf; class 1=1 to 10 RBCs/hpf; class 2=10 to 100 RBCs/hpf; and class=more than 100RBCs/hpf.*

Parameter	Unit	Baseline	4 h	48 h
NAG ratio	U/g	0.53 (0.35)*	0.75 (0.22)	1.43 (0.59)*
GGT ratio	U/g	13.51 (3.28)	15.02 (5.35)	18.19 (6.4)
ALP ratio	U/g	10.05 (9.16)	4.15 (5.27)	9.24 (7.86)
Prot ratio	g/g	0.12 (0.04)	0.10 (0.03)	0.12 (0.08)
RBC	(0-3)	1.00 (1.07)	0.75 (1.17)	1.25 (1.28)
pH		7.0 (1.07)	6.38 (0.74)	6.25 (0.46)
Sp		1.052 (0.01)	1.051 (0.01)	1.041 (0.02)

Table 9 *Results of serum biochemistry measurements of the eight cats presented as mean (±SD). A significant decrease in blood nitrogen is indicated with an asterisk (*, p<0.05)*

Parameter	Unit	Baseline	48 h
Crea	mg/dL	1.70 (0.32)	1.78 (0.29)
Urea	mg/dL	26.05 (7.39)*	23.48 (8.41)*
Alb	g/dL	3.46 (0.16)	3.43 (0.10)
P	mg/dL	3.99 (0.27)	4.00 (0.29)

7. Discussion

The cat is commonly assumed to be similar to a small dog in veterinary medicine with, respect to anatomy and physiology, although it is well-known that this is not always the case. Little is known about the use of CEUS in feline patients. Many elderly cat patients can be kidney compromised, and thus, safety issues are an important area of research in feline medicine. Oftentimes, feline patients need to be sedated or anesthetized; the effect of anesthesia on CEUS is therefore an equally important area of research. The main aim of this thesis was to describe normal organ perfusion in several feline abdominal organs and to establish an imaging protocol specifically suitable for cat patients to serve as a reference for later clinical applications of CEUS. The study approach chosen allowed a broad-spectrum protocol to investigate various aspects of CEUS, and simultaneously opened several options for future experimental and clinical research.

Multiple factors have an influence on the contrast-enhancement of an organ (Porter et al., 1997; Lucidarme et al., 2003; Sonne et al., 2003; Li et al., 2005; 2006; Tang et al., 2007; Mulé et al., 2008; Mulvana et al., 2010). Therefore, thorough assessment of normal organ perfusion and understanding of all of the complex factors influencing perfusion were considered as important first steps prior to conducting clinical studies. Shedding light on the methodology of CEUS and elucidating the basic physics behind it. In CEUS as well as in other diagnostic modalities, there is always a certain learning curve involved in before reaching the full diagnostic value of the modality, which further emphasizes the importance of knowing what is typical for CEUS breed-specifically.

7.1. Normal organ perfusion (I; IV)

In Studies I and IV, typical perfusion patterns for each imaged organ were evident. Perfusion in the abdominal organs of the cat seemed similar to that of the dog based on earlier studies (Ziegler et al., 2003; Nyman et al., 2005; Kamino et al., 2006; Ohlerth et al., 2007a; Waller et al., 2007; Nakamura et al., 2009; Bigliardi et al., 2011; Jiménez et al., 2011). In general, the abdominal organs in the cat seemed to enhance earlier with contrast than in the dog. The enhancement of the spleen was very heterogeneous at the beginning of imaging and it lasted longer than expected from previous reports in dogs (Ohlerth et al., 2007a; Nakamura et al., 2009). However, the cats were imaged under general anesthesia with several anesthetic agents, which may have had an effect on the organ perfusion.

Differences in the functional perfusion parameters between the different organs or differently perfused areas of the kidney and spleen (I; IV), can mostly be explained by physiological differences between the vascular structure and blood flow of the organs (Levesque et al., 1976; Hollenberg et al., 1979; Schmidt et al., 1983; Christensen et al., 1993; Geboes et al., 2001; Pallone et al., 2003; Potdevin et al., 2006; McCuskey et al., 2008). Differences between the organs in the parameters describing the timing (AT, TTP_{inj}, TTP_{inr}), and also in BI and PI (liver and pancreas), are mainly explained by

differences in the afferent vessel systems, vascular structure, and the blood flow (Evans et al., 1993; Christensen et al., 1993; Geboes et al., 2001; McCuskey et al., 2008).

7.1.1. Liver

The liver, which was always imaged first, showed a similar pattern (I) as seen in other species (Ziegler et al., 2003; Nyman et al., 2005; Quaia et al., 2006; Wilson et al., 2007; Li et al., 2006). However, TTP_{inj} seemed to be earlier in the cat (10 s) than in the dog (23-35 s) (Ziegler et al., 2003; Nyman et al., 2005; I). The image quality was not always optimal for the entire liver for two reasons (I). First, the contact between the skin of the cat and the linear probe almost always required a moderate amount of pressure, and despite the pressure there was sometimes lack of contact. This might cause problems, such as a lack of compliance, and thus increased motion and decreased transducer contact in a non-anesthetized animal. Second, the frequency of the probe and the dosage of the contrast media were so high that noticeable attenuation occurred in the far field (4 cm depth).

The relatively large variation detected in liver perfusion parameters (I) is likely to be due to small differences in regional blood flow caused by the complex vascular structure of the liver (Li et al., 2005; 2006; McCuskey et al., 2008), dual blood flow (Lueck et al., 2008), and the close proximity of the diaphragm. This was also considered to be the reason for the increased heterogeneity visible in both the image (during the first 10-15 s) and in the TIC for the entire 30 s. The slope of both the wash-in and wash-out phases was slight as is typical for the liver in other species as well (Ziegler et al., 2003; Li et al., 2005; Nyman et al., 2005; Metoki et al., 2006; Wilson et al., 2007). The broad-shouldered shape of TIC is most likely due to the dual blood flow from the hepatic artery and portal vein (Evans et al., 1993; Lueck et al., 2008), causing constant flow of microbubbles from two vascular systems independently from each other. Furthermore, the gentle and heterogeneous parenchymal and hepatic venous late phase enhancement, is likely to be affected by the travelling of the microbubbles through several capillary beds in the lungs, gastrointestinal tract and liver sinusoids (Evans et al., 1993; McCuskey et al., 2008).

It has been shown previously, that the placement of the transducer and specifically placing the ROI in different liver lobes, has had an effect on the observed perfusion parameters (Li et al., 2006). The placement of the ROI could not be kept constant between the cats in our study (I), and this may have caused overestimation of the variation in the perfusion parameters in the liver data. However, the moderate heterogeneity observed in the perfusion pattern of the liver is reportedly less than the differences between healthy liver and focal neoplastic changes observed by both qualitative and quantitative CEUS (Quaia et al., 2006; Wang et al., 2007; Wilson et al., 2007). Therefore, it is probably not clinically important when comparing focal perfusional changes, but it might be confusing when detecting diffuse or milder focal changes in the liver (Rahbin et al., 2008).

7.1.2. Kidney

The kidney cortex showed a homogeneous, early, and intense enhancement, followed by a more gradual and heterogeneous enhancement of the medulla (I), which was similar to other species (Pietra et al., 2005; Waller et al., 2007; Potdevin et al., 2006) and a previous study in cats (Kinns et al., 2010). However, in our study, TTP_{inj} (6 s) seemed to be earlier in the kidney cortex (I) than in previous studies in cats (13 s) (Kinns et al., 2010) and dogs (13 s) (Waller et al., 2007). The kidney medulla enhanced sparsely, first at the periphery, followed by gradual enhancement of the inner portions (I), according to the blood flow direction (Hollenberg, 1979; Pallone et al., 2003). Nevertheless, TTP_{inj} (22 s) in the medulla in our study (I) corresponded better to the earlier studies in both cats (26 s) (Kinns et al., 2010), and dogs (21 s) (Waller et al., 2007). However, the results from these previous studies (Waller et al., 2007; Kinns et al., 2010) are not entirely comparable with ours due to differences in the anesthetic agents and protocols used (IV). Moreover, possible differences may have existed in the placement and size of the ROIs (II); these differences have been shown to have an effect on perfusion parameters (Schlosser et al., 2001; Verbeek et al., 2001; Potdevin et al., 2006; II). Furthermore, the placement of the ROIs was not reported in the study by Kinns et al. (2010). In addition, the vascular structure has been demonstrated to vary within the kidney cortex (Hollenberg, 1979; Verbeek et al., 2001; Pallone et al., 2003) and therefore differences in the TTP_{inj} may be expected if the placement and size of the ROI are very different.

The marked difference in the perfusion, detected with CEUS, between the kidney cortex and medulla (I) corresponds well with physiology (Hollenberg, 1979; Christensen, 1993; Pallone et al., 2003), and agrees with previous studies in other species (Claudon et al., 1999; Potdevin et al., 2006; Waller et al., 2007) as well as in cats (Kinns et al., 2010). The difference in perfusion between the cortex and medulla may be slightly overestimated in our study (I; II), because the ROIs drawn in the cortex and medulla were not exactly at the same depth. This was due to the small size of the cranial pole of the cat kidney. The depth of the ROI has been shown to have an impact on the obtained signal intensities due to attenuation (Mulé et al., 2008; II). The effect of attenuation was, however, visually estimated to be less than the obvious difference in perfusion between the kidney cortex and medulla. Therefore, respiratory and other motion artifacts occurring in the TICs at the cranial pole of the kidney cortex, could lead to an even more fluctuating TIC, and therefore, to greater variations in the perfusion parameters (II). In addition, if the ROIs were drawn at the same depth (cortical ROI in the cranial pole of the kidney), the size of the ROIs would have been different between the cortex and medulla. This has been shown to have an influence on perfusion parameters as well (Schlosser et al., 2001; II).

The delayed onset of the signal and the longer time required to reach PI (gentler slope) apparent in the kidney medulla (I) compared with the cortex can, therefore, be explained simply by the differences in vascular structure; the majority of the blood flow into the medulla comes from the cortex through a capillary network (Hollenberg, 1979; Christensen, 1993; Pallone et al., 2003). The volume and velocity of the blood flow in the medulla are much less than those in the cortex, and some of the microbubbles have already been exposed to ultrasound before entering the medulla (Potdevin et al., 2006). The large

variation detected in the perfusion parameters of the medulla (I) was also consistent with earlier studies in dogs (Waller et al., 2007), pigs (Claudon et al., 1999), and rabbits (Potdevin et al., 2006) and can be explained by the unique vascular structure of the inner and outer medulla (Pallone et al., 2003). The slower and lower level of blood flow, and therefore, the smaller amount of circulating microbubbles cause more variation in the detected intensities in relation to time (Potdevin et al., 2006), partially due to vascular heterogeneity in the medulla and partially to a greater impact of motion artifact in the TIC. Some of this variation may, however, represent true variation between individuals. Further studies are needed to estimate its importance in clinical patients with renal disease affecting the medulla.

7.1.3. Spleen

Our results indicate that the early parenchymal phase of CEUS splenic perfusion is heterogeneous in healthy cats (IV). The contrast seemed to arrive to the spleen in the cat faster (3-4 s) than in dogs (13 s) (Ohlerth et al., 2007a; IV). However, this is likely to be due to differences in the ROI sizes, which can be expected from the bigger variance in the perfusion parameters in the study by Ohlerth et al. (2007a); The late enhancing areas in the spleen were probably included in the ROI used to calculate the perfusion parameters in the their study. This could explain the slower contrast enhancement, both later arrival of the contrast (AT) and longer time (25 s) required for the spleen to reach peak enhancement (TTP_{inj}) in the dog (Ohlerth et al., 2007a), relative to the early enhancing areas of the spleen in the cat (TTP_{inj} 8 s; IV). Whether these differences are truly species specific or due to differences in the assessment of the perfusion parameters warrants future studies.

The difference detected in our study in the perfusion between the two differently perfused splenic areas (IV) corresponds well with previous research from splenic physiology (Song et al., 1971; Levesque et al., 1976; Schmidt et al., 1982; 1983). However the splenic perfusion in the cat was observed to be more heterogeneous (IV) than in humans (Catalano et al., 2005) or dogs (Ohlerth et al., 2007a; Rossi et al., 2008; Nakamura et al., 2009). Morphological and kinetic studies of the spleen have shown differences in the circulatory pathways between species (Levesque et al., 1976; Schmidt et al., 1983). The nonsinusoidal architecture offers one explanation for the regional delayed enhancement of the splenic parenchyma in our study (IV). However, differences in methodology impair the direct comparison of separate studies in the vascular physiology of the spleen. Furthermore, the effect of physiological stimuli causing splenic contraction or dilatation has not been compared between species. Possible species-specific differences in the blood flow and in the physiological reactions of the spleen may offer an explanation for regional differences in enhancement of the spleen in the cat observed in our study (IV). It may thus explain the longer time to reach homogeneity in the spleen of cats (28 s, in group 1) relative to dogs (approximately 23 s) (Ohlerth et al., 2007a; Rossi et al., 2008; Nakamura et al., 2009). However, the different USCAs and imaging protocols used in the studies might also have an effect on the timing.

7.1.4. Pancreas, small intestine, and mesenteric lymph nodes

The pancreas, small intestine, and mesenteric lymph nodes all showed an early, intense and uniform enhancement (I), as could be expected in organs receiving all of their blood – and therefore also microbubbles – directly from afferent arteries, similarly to other species (Rubaltelli et al., 2004; D'Onofrio et al., 2007; Mitsuoka et al., 2007; Gashen et al., 2010; Jiménez et al., 2011). In comparison with perfusion of medial iliac lymph nodes in dogs (Gashen et al., 2010), both mean AT (cat 4 s vs. dog 6 s) and TTP_{inj} (cat 6 s vs. dog 12-14 s) occurred earlier, however, mean PI (cat 24 dB vs. dog 29 dB) was less, in the mesenteric lymph nodes of the cats (I). This could be due to differences in the afferent vessels, imaging protocol, USCA dose and injection technique, or anesthesia status. Alternatively this might a purely species-specific phenomenon, since a similar tendency was noticed in other organs in our study (I). In addition, the small intestine and mesenteric lymph nodes receive all and the pancreas at least parts of its blood from the cranial mesenteric artery (Schummer et al., 1981a), and thus, similarities in perfusion could be expected based on similarities in circulation. These organs were imaged one after another, and thus the number of USCA doses given was different in the pancreas than in the small intestine and mesenteric lymph nodes (I). However, no differences in the perfusion pattern were observed between the organs (I). Furthermore, the perfusion parameters in the small intestine and mesenteric lymph nodes were highly correlated with each other (I). This also strengthens our results of the repeatability of CEUS between the first and second injections in the liver and kidney cortex (I). In the future, CEUS may prove useful in the assessment of focal and even diffuse changes of these organs, for example in the assessment of pancreatic lesions and, focal mural masses in the intestines or in the search of malignant lymph nodes. Additionally, these organs may even offer a reference for each other, in cases where no normal organ tissue within one of these organs can be found. However, it must be emphasized that some diffuses disease processes, such as lymphoma, may involve both the small intestine and mesenteric lymph nodes, and thus no differences would be expected in the enhancement between the organs.

7.1.5. Repeatability

Repeatability of obtaining perfusional parameters was good in both the liver and renal cortex (I). The difference between the two injections in BI in the liver data (I) could be due to variation caused by respiration, the complex dual and sinusoidal blood flow (Li et al., 2005; Metoki et al., 2006), differences in blood flow between separate areas of the liver (Li et al., 2006) or true baseline variation due to bubble uptake by the sinusoids or bubble saturation (Li et al., 2005). The difference observed in the BI (I) was, however, considered clinically non-significant, since it was markedly less than the reported relative difference in the PI between healthy and neoplastic liver tissue (Hohmann et al., 2003; Bartolotta et al., 2004; Wilson et al., 2007).

In the renal cortex, no significant difference was found between the separate injections in any of the parameters (I). This can be due to the highly vascularized, well-organized structure at the level of both macro- and microcirculation in the kidney cortex (Hollenberg

et al., 1979; Christensen et al. 1993). However, the sequence of the injections was different between the liver and renal cortex (I), as the liver was the first organ imaged (first and second injections) and the cats had already been given repeated injections before the kidney was imaged (fifth and sixth injections). Therefore a small difference in BI between cats could have been hidden by a small amount of residual microbubbles as the effect of several contrast injections on the perfusion parameters and specifically on BI has not been previously reported.

These results indicate that no significant differences in the perfusion parameters existed between two subsequent injections with the scanning intervals used in this study (I). In addition, it seems that the differences would mainly have an effect on the BI (I), and thus, have the greatest effect between the first and second injections, and almost no effect on the following injections, since an attempt was made between each injection to break any residual bubbles. Using multiple injections for each imaging, the comparability between the injections may thus be expected to increase, as the baseline intensity before the injection can be expected to be more similar than between the first and second boluses. In the future, comparison of the first, second, and third injections per organ, in both awake and anesthetized animals in a standardized protocol, might improve the understanding of the differences between separate USCA boluses.

7.1.6. Comparison of different methods in measuring or estimating perfusion

The results from the statistical analyses suggest that the visual estimation of AT from the video only can be considered less sensitive as an analyis method than TIC numerical data and the combination of visual estimation from the video and TIC together. This is probably due to differences in the accuracy of the methods. First, visual estimation from the video has a less sensitive scale (1 s vs. 0.01 s), and second, it is highly dependent on the observer's vision and experience. For clinical use, the three analysis methods can be considered equally accurate and can be used correspondingly, especially when estimating TTP_{inj}, in which no statistically significant differeneces were found between the analyzing methods. The differences in the PI and AT between the analysis of TIC numerical data and the combination of visual estimation from the video and TIC together, suggest that small differences can occur in the perfusion parameters between these methods. However the size of the difference (1dB, < 1s) indicates that the differences are unlikely to be clinically relevant. However, the data and TIC from the kidney cortex is very homogeneous and smooth, and no larger fluctuations occur in the TIC (Figure 3), which would not be the case with the kidney medulla or spleen. Therefore, different results could be expected in a comparison of these methods, when analyzing an organ with more heterogeneous perfusion and large fluctuations in TIC. This must be taken into account when taking these methods into clinical use.

7.2. Importance of location and size of ROI (II)

The well-organized, although complicated vascular structure in the kidney cortex of the cat, provides a good experimental model for quantification of tissue perfusion. In our study, we found that both the depth and the size of the ROI have an effect on the PI (II). The deeper or larger the ROI, the lower the PI (II). This is consistent with previous reports (Sonne et al., 2003; Mulé et al., 2008). The interaction between microbubbles, anatomic structures, and the ultrasound beam is complex, and artifacts complicating the assessment of perfusion may occur, especially in quantitative analyses (Qin et al., 2007; Mulé et al., 2008; Mulvana et al., 2010), although CEUS has excellent sensitivity for microbubble detection and good spatial resolution. The signal intensity is a sum of multiple factors, most of all a sum of ultrasound-induced microbubble behavior. However, multiple factors can have an influence on the detected signal intensity. These include local differences in the replenishment of the contrast agent due to respiratory and other movement; differences in attenuation, both from the microbubbles and the tissues; and unequal destruction of the circulating microbubbles in the whole field-of-view, all of which may vary slightly in the round kidney cortex (Sonne et al., 2003; Mulé et al., 2008). In our studies (I-IV), respiratory and other movement artifacts were estimated to be the most difficult to control, especially in awake cat patients, which can become tachypneic due to stress, causing false peaks and troughs and increased fluctuations into TIC.

The focal zones were consistently placed in the far-field kidney cortex. Despite this, the image quality appeared optimal in the near field-cortex (II). This was most likely due to attenuation in the far field image. The energy of the ultrasound beam and the intensity of tissue contrast enhancement are not constant in the entire imaging field, even in a homogeneous tissue (Sonne et al., 2003; Mulé et al., 2008; Tang et al., 2010). The amount of microbubble destruction and attenuation is dependent on the peak negative pressure focused on the bubbles (Porter et al., 1997; Sonne et al., 2003; Tang et al., 2007), which can be expressed as MI multiplied by the square root of the ultrasound frequency (Miller et al., 2007). The energy of the ultrasound beam is optimized by the ultrasound machine in the focal zone. The amount of energy and therefore attenuation in the imaging field depends mostly on a combination of detection technique (Sonne et al., 2003), transducer frequency (Porter et al., 1997; Tang et al., 2007), frame rate (Porter et al., 1997), MI (Porter et al. 1997; Sonne et al. 2003), dosage (Li et al. 2005) and type of contrast agent (Sonne et al., 2003), amount of overlying tissues between the imaged organ and the transducer (Mulé et al., 2008), distance of the ROI from the focal zone, and the replenishment rate of the bubbles (Lucidarme et al., 2003; Sonne et al., 2003). Furthermore, the cats were given multiple contrast agent injections, which may have caused some level of microbubble saturation, increasing the effect of attenuation in the far field (Skyba et al., 1994; Wei, 2001a; Li et al., 2005). However, in our study (I-IV) the circulating residual microbubbles were broken with B-mode ultrasound between each injection, which can be assumed to prevent or at least diminish the risk of microbubble saturation. Furthermore, no significant differences were found in the perfusion parameters between injections in our study with normal organ perfusion (I).

The kidney cortex is a highly vascularized organ (Hollenberg et al., 1979; Christenssen et al., 1993), and therefore, the number of circulating microbubbles is abundant. We observed relatively high attenuation in the far-field compared with the near-field kidney cortex (I; II). This was thought to be caused by the high transducer frequency (7 MHz), intermediate MI, and placement of the focal zone area in the distal part of the image in combination with microbubble characteristics of the kidney cortex. This is consistent with previous results from USCA Definity® attenuation characteristics with varying transducer frequencies (Goertz et al., 2007).

The size of the ROI was related to the mean PI (II). Increasing the size of the ROI did not, however, decrease the variation in the observed PI (II). Variance between the differently sized ROIs was homogeneous in statistical analysis (II). The small differences in the standard deviation were considered to be caused by noise. This finding conflicts with a previous study (Schlosser et al., 2001), where increased reproducibility in evaluation of replenishment kinetics, in time and intensity parameters, and decreased variation associated with increased ROI size were found in porcine kidneys. However, their study (Schlosser et al., 2001) was ex-vivo, using explanted pig kidneys in a perfusion unit with settings different from ours (II), including continuous infusion of contrast agent, a different transducer frequency and type and larger size differences between the ROIs, which make direct comparison inaccurate. All of these factors have an effect on obtained intensity values and image quality (Porter et al., 1997; Sonne et al., 2003; Li et al., 2005; Tang et al., 2007; Mulé et al., 2008; Talu et al. 2008). Our explanation for the difference we found in the ROI size comparison, is that a larger ROI in the set includes microvascular differences (affecting inflow, outflow and peak intensities), which are not contained in a smaller ROI. Another possibility is that some non-cortical tissue may have been included in the largest ROI.

No statistically significant difference emerged in any perfusion parameter as a function of ROI placement in a row in the near-field cortex (II). This also supports our conclusion of ROI depth and size being the most significant factors affecting signal intensity.

Baseline signal intensity reflects the number of microbubbles in the ROI in the beginning of the wash-in phase. The number of circulating microbubbles (Li et al., 2005), and respiratory and other movement artifacts that cause heterogeneity in the TIC (Mulé et al., 2007) have an influence on the BI. Therefore, the small fluctuations observed in BI in our study (II) are not considered representative of true changes in the kidney perfusion.

No timing parameters were affected by the relative position of ROIs (II), suggesting that the injection protocol is the main factor affecting the timing parameters. These timing parameters may therefore be used clinically, as long as the injection technique is standardized. The magnitude of the measured differences in mean PIs between the ROIs (II) was, however, not large enough to be deemed clinically important. The magnitude of change within individual animals based on depth was greater (II), but not considered clinically important based on the visual image analysis. No quantitative analyses have been done in veterinary medicine with naturally occurring lesions. The lesion characterization with CEUS is based on the subjective visual assessment of the lesion appearance. Further studies are therefore needed to quantitatively investigate the perfusion

in naturally occurring lesions and diffuse parenchymal changes in various organs and disease processes in veterinary patients.

7.3. Effects of anesthesia (I; IV)

Vascular reactions and organ perfusion cannot be easily estimated through cardiopulmonary and blood flow measurements alone. The cardiopulmonary and hemodynamic effects of various anesthetics in cats and other species have been evaluated, but none of the studies have investigated the effects of the anesthetic combinations used in our studies (I, IV). Therefore, we can only speculate on the impact tha the anesthesia used in our study to assess normal organ perfusion had on each separate organ. Furthermore, the time with respect to the equilibrium of the anesthesia was highly different between the first imaged organ (liver) and the last imaged organs (pancreas, small intestine, mesenteric lymph nodes), decreasing the comparability of the results between these organs.

7.3.1. Effect of anesthesia on splenic perfusion (IV)

Our findings suggest that anesthesia increases heterogeneity in the spleen of cats in CEUS (IV). The spleen is commonly observed to become dilated during surgery and the basic ultrasound examinations performed on sedated or anesthetized animals. Many anesthetic agents are known to dilate the spleen and decrease systemic blood pressure, both of which can decrease splenic blood flow. Kinetic research of red cell wash-out from perfused spleens in rats and cats has revealed that the circulatory routes change radically depending on whether the organ is dilated or contracted (Groom et al., 1971; Levesque et al., 1981). Previous studies have investigated the effects of anesthesia on the size of the spleen (Hubbell et al., 1982; O'Brien et al., 2004b; Wilson et al., 2004) as an indicator of splenic congestion.

Acepromazine and thiopental have been shown to cause an ultrasonographic measurable increase in spleen size in dogs (O'Brien et al., 2004b). In another study, the size of the spleen measured surgically was reported to be the largest with ketamine-diazepam or thiopental-induced anesthesia (Wilson et al., 2004). In both earlier studies, the spleen was smallest in dogs treated with propofol (O'Brien et al., 2004b; Wilson et al., 2004), suggesting that propofol induces the mildest dilatation of the spleen relative to the other anesthetic agents (thiopental, acepromazine, ketamine, diazepam) investigated. Conversely, in a previous study by Hubbel et al. (1982), xylazine was found to decrease dose-dependently the size of the spleen via α-adrenergic receptors. In our study (IV), drug-induced splenic congestion may have exaggerated the heterogeneous perfusion patterns in the splenic CEUS. Contrary to previous results of splenic congestion in dogs (O'Brien et al., 2004b), butorphanol and propofol caused more heterogeneity in our study (IV), than a mixture of atropine, acepromazine, xylazine, diazepam, ketamine, and morphine. Interestingly, in an earlier report, propofol was described to decrease the TTP_{inj} of the liver in dogs (Nyman et al., 2005). This may have been due to a propofol-induced increase in the blood flow of the liver (Wouters et al., 1995; Zhu et al., 2008). However, the variation

in the perfusion parameters in the study by Nyman et al. (2005) was large, and this may have had an effect on the comparisons.

The doses of the anesthetic agents are known to have a major role in the hemodynamic effects. Thus, the effects of anesthetic agents can vary depending on the dosage and be different in separate organs such as the liver and the spleen. Whether the increase in heterogeneity of the splenic perfusion in our study (IV) was due to propofol alone, or was a synergistic effect of propofol and butorphanol warrants further investigation. In our study (IV), the depth and duration of anesthesia varied between groups (1 and 2anesth), which may have had an influence on the congestive effects of the spleen (Kramer et al., 1951; Guntheroth et al., 1963). Furthermore, the interaction of several simultaneous stimuli and different drugs on splenic circulation can be considered unpredictable. Thus, the neutering procedure may also have had an impact on the hemodynamic balance via sympathetic stimulation, and even directly on the spleen in group 1.

In our study, neither of the anesthesia protocols was found to influence the timing of heterogeneity or the time to the spleen being considered homogeneous, even when different equipment was used (IV). This further supports the evidence that the regional differences in perfusion of the spleen are due to physiological differences in the blood flow within separate regions of the spleen, which seem to be affected by the anesthesia protocols chosen. Probably the heterogeneity of the spleen was overestimated in the first study (group 1), when combinent injection anesthesia protocol was used (IV). However, as the comparison of the spleen in awake and anesthetized cats (groups 2awake and 2anesth) demonstrated, some degree of heterogeneity can be expected even in awake animals (IV).

Anesthesia was, nevertheless, found to have an effect on the AT_v in visual estimation between the cat groups 2awake and 2anesth (IV), as might be expected from anesthetic agents (propofol and butorphanol) that have negative effects on cardiac output, systemic vascular resistance, and mean arterial pressure (Muir et al., 2007). Similar effects can be anticipated in CEUS of other organs as well, when animals are sedated or anesthetized with anesthetic agents having similar effects on systemic circulation. Based on our results (IV), the impact of anesthesia should, however, be taken into account when imaging the feline spleen. Further studies are required to determine the clinical significance of the described findings, and to identify an optimal anesthesia protocol for use in veterinary patients in CEUS.

7.4. Effect of CEUS on kidneys (III)

The minor changes in the urinary NAG ratio detected in our study were considered clinically insignificant (III), because the maximal values were still within the range reported earlier for healthy cats (Uechi et al., 1994b; 1998; Sato et al., 2002b; Narita et al., 2005; Lapointe et al., 2008; Brunker et al., 2009; Jepson et al., 2009) and less than has been reported to be indicative of AKI in dogs and cats (Heiene et al., 1991; Uechi et al., 1994a; Sato et al., 2002a; 2002b). The magnitude of the change and the maximal values of the NAG ratio (III) were also lower than those found to be normal circadian variation in healthy cats (Uechi et al., 1998).

For consistency, sample collection, storage times and conditions, and analysis procedures were kept constant throughout our study (III). To avoid depletion of enzymes, ALP and GGT activities were measured within 4 h of urine collection, and NAG activity was measured after 1 month of storage at -80°C, which has been shown to be an acceptable practice in human medicine (Mueller et al., 1986). Urinary enzyme activities vary depending on storage conditions and analysis procedures (Gossett et al., 1987; Matteucci et al., 1994). Enzymes may become inactivated or unstable due to unfavorable conditions (Jung et al., 1982; Bondiou et al., 1985; Mueller et al., 1986; Matteucci et al., 1991). However, the results from previous studies have been contradictory concerning the stability of urinary enzymes (Jung et al., 1982; Bondiou et al., 1985; Gossett et al., 1987; Pocsi et al., 1990; Matteucci et al., 1991; 1994). Major factors affecting enzyme stability include storage time and temperature. In addition, the quality of the urine sample and, the presence of blood cells, feces or bacteria may also have an effect on urinary enzyme activities (Raab, 1972).

Urine enzyme-to-creatinine ratios in spot samples have been shown to correlate well with 24 h enzyme excretion (Gossett et al., 1987; Uechi et al. 1994b; 1998; Grauer et al., 1995). Thus, collection of urine over a 24 h period was not considered necessary in our study, and cystocentesis was chosen as the method of urinary collection to maintain appropriate sample timing (III).

Elevated urinary enzyme activities, specifically the NAG ratio, can either indicate tubular cellular damage in the kidney or reflect increased lysosomal cellular acitivity without cellular damage (Trof et al., 2006; Liangos et al., 2007). This further supports our conclusion that the mild rise after 48 h in NAG ratio (III) can be considered clinically of low importance with regard to detecting AKI. However, the number of animals in the study was small, and adverse effects with very low prevalence cannot be ruled out by this study. Nevertheless, no evidence of clinically significant kidney injury caused by CEUS using low to intermediate MI has emerged in earlier studies in humans or pigs (Piscaglia et al., 2006; Jiménez et al., 2008). A possible explanation for the contradictory results between previous studies is differences in imaging parameters. Further studies are therefore warranted to seek evidence of hematuria in clinical patients with impaired kidney function and CEUS with moderate MI (higher than used in Study III).

While hematuria was detected in the samples, no significant increase in the degree was observed. Collecting urine by cystocetesis potentially caused some bleeding (III), which might be a confounding factor, particularly considering the fact that hematuria may influence the urine enzyme-to-creatinine ratio (Grauer et al., 1995; Brunker et al., 2009). Cystocentesis was chosen as the method of urinary collection to be consistent (the same method each time), to avoid contamination with bacteria or enzyme additions from distal urinary tract or gonadal secretions, to avoid long urine collection periods that could cause depletion of enzyme activities, and to obtain the urine samples at exactly same time-points from each cat in relation to the contrast ultrasound (III). In rodents, hematuria after CEUS was significantly reduced by 24 h post-CEUS (Williams et al., 2007), and thus, our goal was to collect urine at certain timepoints before and after the expected decrease of possible transient hematuria.

The decrease in the BUN (III) was not considered clinically significant because possible kidney injuries are rather expected to increase BUN, if change at all, after contrast ultrasound. Also, the magnitude of change was considered to be clinically insignificant (III). Some of the cats had already mildly elevated BUN and plasma creatinine concentrations before the study, which was interpreted to be due to a protein-rich diet during the study, catabolism (the cats had been given a slimming diet), and possible sub-clinical dehydration due to sedation for the permanent cathether placement (III). The BUN and creatinine concentrations did not increase in any of the animals, and the urine specific gravity was within normal limits, suggesting adequate kidney function. Both BUN and creatinine concentrations are considered to be poor markers for acute kidney injury because of renal reserve and numerous non-renal influencing factors (race, age, gender, muscle metabolism, protein intake, drugs, total body volume) (Watson et al., 1981; Finco, 1997; Trachtenberg et al, 2007).

Urine pH has been reported to have an influence on urinary enzyme activities (Jung et al., 1982; Uechi et al., 1994b; Brunker et al., 2009). At very low (4.7) or very high (8.0) urine pH-values, the enzymes may become inactivated or unstable (Jung et al., 1982). In our study, the urine pH was deemed suitable for urine enzyme activity measurements. In four of the animals studied, the urine pH was at its higher limits (pH 8.0) in the samples collected before CEUS. In a recent study on dogs (Brunker et al., 2009), urine pH was found to have an effect on urine GGT ratio, but not on urine NAG ratio. At pH $\geq$ 7.0, the mean urine GGT ratio increased almost twofold and the mean urine NAG ratio decreased, but not significantly (Brunker et al., 2009). Based on earlier studies, the baseline GGT activities may have been slightly underestimated by the relatively high urine pH in our study (III).

In Study III the transducer frequency, contrast agent dosing and imaging settings were selected to mimic clinical conditions as realistically as possible. The study was performed under conditions intended to enable the occurrence of possible bioeffects based on results from earlier experimental laboratory studies (Williams et al., 2007; Miller et al., 2008). In previous studies, kidney injuries were observed with limited transducer frequency range of 1.5-3.2 MHz (Miller et al., 2008). The threshold for occurrence of kidney injury has been observed to increase linearly with increasing MIs and frequencies (Miller et al., 2008). Excessive post-marketing surveys have revealed no such effect in man (Piscaglia et al., 2006). Contrary to the studies performed by Miller et al. (2007; 2008; 2009; 2010) with rats, mice, and pigs, in a recent study no evidence of kidney damage emerged in either histopathological or laboratory analyses after CEUS of surgically exposed pig kidneys (Jiménez et al., 2008) with low to intermediate MI (0.2-0.5) and continuous imaging, but a high MI (1.9) was used to destruct residual microbubbles. In our study (III), the transducer frequency (3 MHz) and the imaging protocol and duration were similar, but the MI was lower than in the experimental studies during the actual imaging because of the clinical imaging settings. However, high MI (conventional B-mode) was used in Study III to destroy residual microbubbles before imaging the kidney due to prior imaging of the spleen, which may have further increased the potential risk of kidney cellular injury induced by CEUS. Therefore, CEUS can be assumed to be safe for use in imaging kidney lesions. In conclusion, CEUS can be considered to at least be the safest contrast imaging

modality for kidney-compromised patients compared with contrast-enhanced CT and MRI, which have proven to have harmful effects on kidneys (Mehran et al., 2006; Persson et al., 2006; Perazella, 2008). However, further studies are needed to assess the effects of CEUS in older animals and in patients with impaired kidney function.

7.5. Limitations of the studies

Little is known of the exact effects of anesthesia on the perfusion of various organs. Anesthesia has been previously reported to have an effect on perfusion parameters in CEUS of the liver (Nyman et al., 2005). In our study, the impact of multi-injection balanced anesthesia on organ perfusion can thus be considered a confounding factor in the assessment of normal organ perfusion (I), and warrants detailed investigations. Furthermore, the exact effects of the various anesthetic agents given in the study in each imaged organ as a function of time are not known. Despite anesthesia, equal perfusion parameters were found between the pancreas, small intestine, and mesenteric lymph nodes, indicating similar tendencies (I).

In the comparison of splenic perfusion between cat groups, differences in the equipment, and thus, in the imaging protocol, and especially in the transducer frequency, were thought to be a confounding factor (IV). This may have influenced the subjective assessment of the image between groups 1 and 2 (IV). Estimation of homogeneity between groups 1 and 2 was difficult due to differences in the pixel size of the image between the machines. Estimation of enhancement homogeneity was, however, deemed an important aspect for future clinical studies. This raises a question of CEUS in general; how small can the focal changes be and still be visualized by CEUS, depending on the spatial image resolution, and therefore, mainly on equipment? In addition to the differences in the imaging, the cats in groups 1 and 2 were different in the splenic study (IV), which may hinder the comparison of the two differently anesthetized groups 1 and 2. However, the variation caused by differences between the two groups of cats can be considered a strength of the study since the major clinical finding, the heterogeneity of the cat spleen, was evident despite these confounding factors (IV).

8. Conclusions

1. Our results indicate that CEUS can be used to estimate organ perfusion in cats, as in other species. The obtained baseline data in these studies can serve as reference values in the future assessment of clinical feline patients with kidney, liver, pancreatic, intestinal, or lymph node disease, or suspected vascular compromise.

2. Quantitative CEUS, however, results very often in values that are not entirely comparable between studies. The results may vary due to the multiple factors affecting TIC. For perfusion quantification, the ROI should be selected based on where the enhancement is the most homogeneous and close to the focal zone range. The ROI size should be large enough to represent the tissue being analyzed, but small enough to avoid surrounding structures and vessels. When comparing two different ROIs in a patient with focal lesions, the ROIs should be placed at the same depth and be as similar in size as possible. Moreover, the timing parameters appear to be independent of ROI size and placement and are therefore applicable for clinical imaging.

3. Our study suggests that CEUS can be used for analyzing kidney perfusion in feline patients with minimal risks of cellular damage in kidneys. It is recommended that the exposure (contrast dosing, MI, scanning time) should be kept to the minimum required for diagnostic imaging.

4. This study emphasizes that the estimation of focal perfusion defects in CEUS of the spleen in cats should be performed with caution, and only after disappearance of the initial heterogeneity. Based on our results, the effect of anesthesia should also be taken into account when imaging the feline spleen.

References

Abramowicz, J.S., Barnett, S.B., Duck, F.A., Edmonds, P.D., Hynynen, K.H., Ziskin, M.C., 2008. Fetal thermal effects of diagnostic ultrasound. J. Ultrasound Med. 27, 541-559.

Albrecht, T., Hoffmann, C.W., Schettler, S., Overberg, A., Ilg, M., von Behren, P.L., Bauer, A., Wolf, K.J., 2000. B-Mode enhancement at phase-inversion US with air-based microbubble contrast agent: Initial experience in humans. Radiology 216, 273-278.

Arditi, M., Brenier, T., Schneider, M., 1997. Preliminary study in differential contrast echography. Ultrasound Med. Biol. 23, 1185-1194.

Bartolotta, T.V., Midiri, M., Scialpi, M., Sciarrino, E., Galia, M., Lagalla, R., 2004. Focal nodular hyperplasia in normal and fatty liver: A qualitative and quantitative evaluation with contrast-enhanced ultrasound. Eur. Radiol. 14, 583-591.

Bauer, A., Solbiati, L., 2003. Ultrasound contrast agents. In: Solbiati, L., Martegani, A., Leen, E. et al (Ed.), Contrast-Enhanced Ultrasound of Liver Diseases. Springer-Verlag, Milan, 21-26.

Bazzi, C., Petrini, C., Rizza, V., Arrigo, G., Napodano, P., Paparella, M., D'Amico, G., 2002. Urinary N-acetyl-beta-glucosaminidase excretion is a marker of tubular cell dysfunction and a predictor of outcome in primary glomerulonephritis. Nephrol. Dial. Transplant. 17, 1890-1896.

Bertolotto, M., Martegani, A., Aiani, L., Zappetti, R., Cernic, S., Cova, M.A., 2008. Value of contrast-enhanced ultrasonography for detecting renal infarcts proven by contrast enhanced CT. A feasibility study. Eur. Radiol. 18, 376-383.

Bigliardi, E., Ferrari, L., 2011. Contrast-enhanced ultrasound of the normal canine prostate gland. Vet. Radiol. Ultrasound 52, 107-110.

Blomley, M., Albrecht, T., Cosgrove, D., Jayaram, V., Butler-Barnes, J., Eckersley, R., 1998. Stimulated acoustic emission in liver parenchyma with Levovist. Lancet 351, 568.

Blomley, M., Claudon, M., Cosgrove, D., 2007. WFUMB safety symposium on ultrasound contrast agents: Clinical applications and safety concerns. Ultrasound Med. Biol. 33, 180-186.

Bondiou, M.T., Bourbouze, R., Bernard, M., Percheron, F., Perez-Gonzalez, N., Cabezas, J.A., 1985. Inhibition of A and B N-acetyl-beta-D-glucosaminidase urinary isoenzymes by urea. Clin. Chim. Acta 149, 67-73.

Bouakaz, A., de Jong, N., Cachard, C., Jouini, K., 1998. On the effect of lung filtering and cardiac pressure on the standard properties of ultrasound contrast agent Ultrasonics 36, 703-708.

Bouakaz, A., Versluis, M., de Jong, N., 2005. High-speed optical observations of contrast agent destruction. Ultrasound Med. Biol. 31, 391-399.

Bouakaz, A., de Jong, N., 2007. WFUMB safety symposium on echo-contrast agents: Nature and types of ultrasound contrast agents. Ultrasound Med. Biol. 33, 187-196.

Brunker, J.D., Ponzio, N.M., Payton, M.E., 2009. Indices of urine N-acetyl-beta-D-glucosaminidase and gamma-glutamyl transpeptidase activities in clinically normal adult dogs. Am. J. Vet. Res. 70, 297-301.

Bude, R.O., 2004. Does contrast-enhanced US have potential for sentinel lymph node detection? Radiology 230, 603-604.

Calliada, F., Campani, R., Bottinelli, O., Bozzini, A., Sommaruga, M.G., 1998. Ultrasound contrast agents: Basic principles. Eur. J. Radiol. 27, 157-160.

Catalano, O., Sandomenico, F., Matarazzo, I., Siani, A., 2005. Contrast-enhanced sonography of the spleen. AJR Am. J. Roentgenol. 184, 1150-1156.

Chaudhari, M.H., Forsberg, F., Voodarla, A., Saikali, F.N., Goonewardene, S., Needleman, L., Finkel, G.C., Goldberg, B.B., 2000. Breast tumor vascularity identified by contrast enhanced ultrasound and pathology: Initial results. Ultrasonics 38, 105-109.

Chen, S., Kroll, M.H., Shohet, R.V., Frenkel, P., Mayer, S.A., Grayburn, P.A., 2002. Bioeffects of myocardial contrast microbubble destruction by echocardiography. Echocardiography 19, 495-500.

Chomas, J., Dayton, P., May, D., Ferrara, K., 2002. Nondestructive subharmonic imaging. IEEE Trans. Ultrason. Ferroelec. Freq. Contr. 49, 883-892.

Church, C.C., 1995. The effects of an elastic solid surface layer on the radial pulsations of gas bubbles. J. Acoust. Soc. Am. 97, 1510-1521.

Christensen, G., 1993. The urogenital apparatus. In: Evans, H., Christensen, G. (Ed.), Miller's anatomy of the dog. WB Saunders, Philadelphia, 544-554.

Claudon, M., Barnewolt, C.E., Taylor, G.A., Dunning, P.S., Gobet, R., Badawy, A.B., 1999. Renal blood flow in pigs: Changes depicted with contrast-enhanced harmonic US imaging during acute urinary obstruction. Radiology 212, 725-731.

Claudon, M., Cosgrove, D., Albrecht, T., Bolondi, L., Bosio, M., Calliada, F., Correas, J.M., Darge, K., Dietrich, C., D'Onofrio, M., Evans, D.H., Filice, C., Greiner, L., Jäger, K., Jong, N., Leen, E., Lencioni, R., Lindsell, D., Martegani, A., Meairs, S., Nolsoe, C., Piscaglia, F., Ricci, P., Seidel, G., Skjoldbye, B., Solbiati, L., Thorelius, L., Tranquart, F., Weskott, H.P., Whittingham, T., 2008. Guidelines and good clinical practice recommendations for contrast enhanced ultrasound (CEUS) - Update 2008. Ultraschall in Med. 29, 28-44.

Clemo, F.A., 1998. Urinary enzyme evaluation of nephrotoxicity in the dog. Toxicol. Pathol. 26, 29-32.

Coca, S.G., Yalavarthy, R., Concato, J., Parikh, C.R., 2008. Biomarkers for the diagnosis and risk stratification of acute kidney injury: A systematic review. Kidney Int. 73, 1008-1016.

Cochran, S.T., Bomyea, K., 2002. Trends in adverse events from iodinated contrast media. Acad. Radiol. 9, 65-68.

Corral, J., Miralles, J.M., Garcia-Pascual, I.J., Corrales, J.J., Garcia-Sastre, A., Villar, E., 1992. Increased serum N-acetyl-beta-D-glucosaminidase and alpha-D-mannosidase activities in obese subjects. Clin. Investig. 70, 880-884.

Correas, J.M., Claudon, M., Tranquart, F., Hélénon, O., 2006. The kidney: Imaging with microbubble contrast agents. Ultrasound Q. 22, 53-66.

Cosgrove, D., 1997. Echo enhancers and ultrasound imaging. Eur. J. Radiol. 26, 64-76.

Cosgrove, D., 2004. Editorial. Eur. Radiol. 14, 1-3.

Cosgrove, D., 2006. Ultrasound contrast agents: An overview. Eur. J. Radiol. 60, 324-330.

Dalecki, D., 2007. WFUMB safety symposium on echo-contrast agents: Bioeffects of ultrasound contrast agents in vivo. Ultrasound Med. Biol. 33, 205-213.

D'Amico, G., Bazzi, C., 2003. Urinary protein and enzyme excretion as markers of tubular damage. Curr. Opin. Nephrol. Hypertens. 12, 639-643.

Darge, K., Troeger, J., 2002. Vesicoureteral reflux grading in contrast-enhanced voiding urosonography. Eur. J. Radiol. 43, 122-128.

de Jong, N., Cornet, R., Lancee, C.T., 1994a. Higher harmonics of vibrating gas-filled microspheres. Part one: Simulations. Ultrasonics 32, 447-453.

de Jong, N., Cornet, R., Lancee, C.T., 1994b. Higher harmonics of vibrating gas-filled microspheres. Part two: Measurements. Ultrasonics 32, 455-459.

de Jong, N., Frinking, P.J., Bouakaz, A., Ten Cate, F.J., 2000. Detection procedures of ultrasound contrast agents. Ultrasonics 38, 87-92.

de Jong, N., Bouakaz, A., Frinking, P.J., Ten Cate, F.J., 2001. Contrast-specific imaging modes. In: Goldberg, B.B, Raichlen, J.S., Forsberg, F. (Ed.), Ultrasound Contrast Agents. Basic Principles and Clinical Applications. Martin Dunitz Ltd., United Kingdom, 25-36.

de Jong, N., Bouakaz, A., Frinking, P., 2002. Basic acoustic properties of microbubbles. Echocardiography 19, 229-240.

de Jong, N., Emmer, M., Chin, C.T., Bouakaz, A., Mastik, F., Lohse, D., Versluis, M., 2007. "Compression-only" behavior of phospholipid-coated contrast bubbles. Ultrasound Med. Biol. 33, 653-656.

de Jong, N., Emmer, M., van Wamel, A., Versluis, M., 2009. Ultrasonic characterization of ultrasound contrast agents. Med. Biol. Eng. Comput. 47, 861–873.

Dijkmans, P.A., Visser, C.A., Kamp, O., 2005. Adverse reactions to ultrasound contrast agents: Is the risk worth the benefit? Eur. J. Echocardiogr. 6, 363-366.

Dong, F., Madsen, E.L., MacDonald, M.C., Zagzebski, J.A., 1999. Nonlinearity parameter for tissue-mimicking materials. Ultrasound Med. Biol. 25, 831-838.

D'Onofrio, M., Martone, E., Malago, R., Faccioli, N., Zamboni, G., Comai, A., Cugini, C., Gubello, T., Pozzi Mucelli, R., 2007. Contrast-enhanced ultrasonography of the pancreas. J. Pancreas 8, 71-76.

Drobac, M., Gilbert, B., Howard, R., Baigrie, R., Rakowski, H., 1983. Ventricular septal defect after myocardial infarction: Diagnosis by two-dimensional contrast echocardiography. Circulation 67, 335-341.

Du, J., Li, F.H., Fang, H., Xia, J.G., Zhu, C.X., 2008. Correlation of real-time gray scale contrast-enhanced ultrasonography with microvessel density and vascular endothelial growth factor expression for assessment of angiogenesis in breast lesions. J. Ultrasound Med. 27, 821-831.

EMEA 2005, SonoVue,

http://www.ema.europa.eu/ema/index.jsp?curl=pages/medicines/human/medicines/000303/human_med_001059.jsp&murl=menus/medicines/medicines.jsp&mid=WC0b01ac058001d125, 22.10.2010

EPAR 2005, SonoVue, Assesment history, Scientific discussion 21/10/2005,

http://www.ema.europa.eu/docs/en_GB/document_library/EPAR-_Scientific_Discussion/human/000303/WC500055376.pdf, 22.10.2010

EPAR 2008, SonoVue, Product information 21/02/2008,

http://www.ema.europa.eu/docs/en_GB/document_library/EPAR_-_Product_Information/human/000303/WC500055380.pdf, 22.10.2010

Emmer, M., van Wamel, A., Goertz, D.E., de Jong, N., 2007. The onset of microbubble vibration. Ultrasound Med. Biol. 33, 941-949.

Emmer, M., Vos, H.J., Goertz, D.E., van Wamel, A., Versluis, M., de Jong, N., 2009. Pressure-dependent attenuation and scattering of phospholipid-coated microbubbles at low acoustic pressures. Ultrasound Med. Biol. 35, 102-111.

Evans, H., Christensen, G., 1993. Digestive apparatus and abdomen. In: Evans, H., Christensen, G. (Ed.), Miller's anatomy of the dog. WB Saunders, Philadelphia, 479-484.

FDA 2001, Drug Approval Package,

http://www.accessdata.fda.gov/drugsatfda_docs/nda/2001/21-064_Definity.cfm, 22.10.2010

FDA 2008, Labeling Revision

http://www.accessdata.fda.gov/drugsatfda_docs/label/2008/021064s009lbl.pdf, 22.10.2010

Finco, D.R., 1997. Kidney Function: VI Tests of Renal Function. In: Kaneko, J.J., Harvey, J.W., Bruss, M.L. (Ed.), Clinical Biochemistry of Domestic Animals. Academic Press, San Diego, 468-480.

Fleischer, A.C., Lyshchik, A., Jones, H.W., Crispens, M., Loveless, M., Andreotti, R.F., Williams, P.K., Fishman, D.A, 2008. Contrast-enhanced transvaginal sonography of benign versus malignant ovarian masses: Preliminary findings. J. Ultrasound Med. 27, 1011-1018.

Forsberg, F., Wu,Y., Makin, I.R., Wang,W., Wheatley,M.A., 1997. Quantitative acoustic characterization of a new surfactant-based ultrasound contrast agent. Ultrasound Med. Biol. 23, 1201-1208.

Forsberg, F., Shi, W.T., 2001. Physics of contrast-microbubbles. In: Goldberg, B.B, Raichlen, J.S., Forsberg, F. (Ed.), Ultrasound Contrast Agents. Basic Principles and Clinical Applications. Martin Dunitz Ltd., United Kingdom, 15-24.

Friedrich-Rust, M., Schneider, G., Bohle, R.M., Herrmann, E., Sarrazin, C., Zeuzem, S., Bojunga, J., 2008. Contrast-enhanced sonography of adrenal masses: Differentiation of adenomas and nonadenomatous lesions. AJR Am. J. Roentgenol. 191, 1852-1860.

Frinking, P.J., de Jong, N., 1998. Acoustic modeling of shell-encapsulated gas bubbles. Ultrasound Med. Biol. 24, 523-533.

Frinking, P.J., Cespedes, E.I., Kirkhorn, J., Torp, H.G., de Jong, N., 2001. A new ultrasound contrast imaging approach based on the combination of multiple imaging pulses and a separate release burst. IEEE Trans. Ultrason. Ferroelec. Freq. Contr. 48, 643-651.

Frush, D.P., Babcock, D.S., White, K.S., Barr, L.L., 1995. Quantification of intravenous contrast-enhanced Doppler power spectrum in the rabbit carotid artery. Ultrasound Med. Biol. 21, 41-47.

Fujita, H., Narita, T., Morii, T., Shimotomai, T., Yoshioka, N., Kakei, M., Ito, S., 2002. Increased urinary excretion of N-acetylglucosaminidase in subjects with impaired glucose tolerance. Ren. Fail. 24, 69-75.

Garry, F., Chew, D.J., Hoffsis, G.F., 1990. Enzymuria as an index of renal damage in sheep with induced aminoglycoside nephrotoxicosis. Am. J. Vet. Res. 51, 428-432.

Gashen, L., Angelette, N., Stout, R., 2010. Contrast-enhanced ultrasonography of medial iliac lymph nodes in healthy dogs. Vet. Radiol. Ultrasound 51, 634-637.

Geboes, K., Geboes, K.P., Maleux, G., 2001. Vascular anatomy of the gastrointestinal tract. Best Pract. Res. Clin. Gastroenterol. 15, 1-14.

Girard, M.S., Mattrey, R.F., Baker, K.G., Peterson, T., Deiranieh, L.H., Steinbach, G.C., 2000. Comparison of standard and second harmonic B-Mode sonography in the detection of segmental renal infarction with sonographic contrast in a rabbit model. J. Ultrasound Med. 19, 185-192.

Goertz, D.E., de Jong, N., van der Steen, A.F., 2007. Attenuation and size distribution measurements of Definity and manipulated Definity populations. Ultrasound Med. Biol. 33, 1376-1388.

Gorce, J.M., Arditi M., Schneider M., 2000. Influence of bubble size distribution on the echogenicity of ultrasound contrast agents. A study of SonoVue. Invest. Radiol. 35, 661–671.

Görg, C., 2007. The forgotten organ: Contrast enhanced sonography of the spleen. Eur. J. Radiol. 64, 189-201.

Gossett, K.A., Turnwald, G.H., Kearney, M.T., Greco, D.S., Cleghorn, B., 1987. Evaluation of gamma-glutamyl transpeptidase to creatinine ratio from spot samples of urine supernatant, as an indicator of urinary enzyme excretion in dogs. Am. J. Vet. Res. 48, 455-457.

Gramiak, R., Shah, P.M., 1968. Echocardiography of the aortic root. Invest. Radiol. 3, 356-366.

Grauer, G.F., Greco, D.S., Behrend, E.N., Mani I., Fettman, M.J., Allen, T.A., 1995. Estimation of quantitative enzymuria in dogs with gentamicin-induced nephrotoxicosis using urine enzyme/creatinine ratios from spot urine samples. J. Vet. Intern. Med. 9, 324-327.

Greco, D.S., Turnwald, G.H., Adams, R., Gossett, K.A., Kearney, M., Casey, H., 1985. Urinary gamma-glutamyl transpeptidase activity in dogs with gentamicin-induced nephrotoxicity. Am. J. Vet. Res. 46, 2332-2335.

Greis, C., 2004. Technology overview: Sonovue (Bracco, Milan). Eur. Radiol. 14, 11-15.

Groom, A.C., Song, S.H., 1971. Effects of norepinephrine on washout of red cells from the spleen. Am. J. Physiol. 221, 255-258.

Guntheroth, W.G., Mullins, G.L., 1963. Liver and spleen as venous reservoirs. Am. J. Physiol. 204, 35-41.

Han, W.K., Waikar, S.S., Johnson, A., Betensky, R.A., Dent, C.L., Devarajan, P., Bonventre, J.V., 2008. Urinary biomarkers in the early diagnosis of acute kidney injury. Kidney Int. 73, 863-869.

Haers, H., Vignoli, M., Paes, G., Rossi, F., Taeymans, O., Daminet, S., Saunders, J.H., 2010. Contrast harmonic ultrasonographic appearance of focal space-occypying renal lesions. Vet. Radiol. Ultrasound 50, 188-194.

Hardy, M.L., Hsu, R.C., Short, C.R., 1985. The nephrotoxic potential of gentamicin in the cat: Enzymuria and alterations in urine concentrating capability. J. Vet. Pharmacol. Ther. 8, 382-392.

Harmankaya, O., Ozturk, Y., Basturk, T., Obek, A., 2001. Urinary excretion of N-acetyl-beta-D-glucosaminidase in newly diagnosed essential hypertensive patients and its changes with effective antihypertensive therapy. Int. Urol. Nephrol. 32, 583-584.

Heiene, R., Biewenga, W.J., Koeman, J.P., 1991. Urinary alkaline phosphatase and γ-glutamyl transferease as indicators of acute renal damage in dogs. J. Small Anim. Pract. 32, 521-524.

Heiene, R., Moe, L., Molmen, G., 2001. Calculation of urinary enzyme excretion, with renal structure and function in dogs with pyometra. Res. Vet. Sci. 70, 129-137.

Hoff, L., 1996. Acoustic properties of ultrasonic contrast agents. Ultrasonics 34, 591-593.

Hoff, L., Sontum, P., Hovem, J., 2000. Oscillations of polymeric microbubbles: Effect of the encapsulatings. J. Acoust. Soc. Am. 107, 2272-2280.

Hohmann, J., Albrecht, T., Hoffmann, C.W., Wolf, K.J., 2003. Ultrasonographic detection of focal liver lesions: Increased sensitivity and specificity with microbubble contrast agents. Eur. J. Radiol. 46, 147-159.

Hollenberg, N., 1979. The physiology of the renal circulation. In: Black D, Jones N, editors. Renal Disease. (Ed.), Oxford, England: Blackwell Mosby Book Distributions, 30-63.

Hubbell, J.A., Muir, W.W., 1982. Effect of xylazine hydrochloride on canine splenic weight: An index of vascular capacity. Am. J. Vet. Res. 43, 2188-2192.

Iqbal, M.P., Ali, A.A., Waqar, M.A., Mehboobali, N., 1998. Urinary N-acetyl-beta-D-glucosaminidase in rheumatoid arthritis. Exp. Mol. Med. 30, 165-169.

Iqbal, M.P., Kazmi, K.A., Jafri, H.R., Mehboobali, N., 2003. N-acetyl-beta-D-glucosaminidase in acute myocardial infarction. Exp. Mol. Med. 35, 275-278.

Ivancic, M., Long, F., Seiler, G.S., 2009. Contrast harmonic ultrasonography of splenic masses and associated liver nodules in dogs. J. Am. Vet. Med. Assoc. 234, 88-94.

Jäger, K., Judmaier, G., Mertz, E., Seitz, K., 2004. EFSUMB study group: Guidelines for the use of contrast agents in ultrasound. Ultrashall in Med. 2004; 25:249-256.

Jepson, R.E., Brodbelt, D., Vallance, C., Syme, H.M., Elliott, J., 2009. Evaluation of predictors of the development of azotemia in cats. J. Vet. Intern. Med. 23, 806-813.

Jiménez, C., de Gracia, R., Aguilera, A., Alonso, S., Cirugeda, A., Benito, J., Regojo, R.M., Aguilar, R., Warlters, A., Gomez, R., Largo, C., Selgas, R., 2008. In situ kidney insonation with microbubble contrast agents does not cause renal tissue damage in a porcine model. J. Ultrasound Med. 27, 1607-1615.

Jiménez, D.A., O'Brien, R.T., Wallace, J.D., Klocke, E., 2011. Intraoperative contrast-enhanced ultrasonography of normal canine jejunum. Vet. Radiol. Ultrasound, in press.

Johnson-Neitman, J.L., O'Brien, R.T., Wallace, J.D., 2007. Quantitative perfusion analysis of the normal canine pancreas and duodenum using contrast-enhanced ultrasound, congress abstract, ACVR Annual Scientific Meeting, November 28, Chicago, Illinois.

Jung, K., Pergande, M., Schroder, K., Schreiber, G., 1982. Influence of pH on the activity of enzymes in urine at 37 degrees C. Clin. Chem. 28, 1814.

Kaler, L.W., Haensly, W.E., 1978. Kidney in the aging cat: Hexokinase, aldolase, L-alpha-glycerophosphate dehydrogenase, and lactate dehydrogenase histochemistry. Am. J. Vet. Res. 39, 1331-1336.

Kanemoto, H., Ohno, K., Nakashima, K., Takahashi, M., Fujino, Y., Nishimura, R., Tsujimoto, H., 2009. Characterization of canine focal liver lesions with contrast-enhanced ultrasound using a novel contrast agent-sonazoid. Vet. Radiol. Ultrasound 50, 188-194.

Kamino, D., Hata, J., Haruma, K., Manabe, N., Tanaka, S., Chayama, K., 2006. Real-time visualization and quantitation of canine gastric mucosal blood flow by contrast-enhanced ultrasonography. Scand. J. Gastroenterol. 41, 856-861.

Karaman, C.Z., Unsal, A., Akdilli, A., Taskin, F., Erol, H., 2005. The value of contrast enhanced power Doppler ultrasonography in differentiating hypoehoic lesions in the peripheral zone of prostate. Eur. J. Radiol. 54, 148-155.

Katayama, H., 1990a. Adverse reactions to contrast media. What are the risk factors? Invest.Radiol. 25, 16-17.

Katayama, H., Yamaguchi, K., Kozuka, T., Takashima, T., Seez, P., Matsuura, K., 1990b. Adverse reactions to ionic and nonionic contrast media. A report from the Japanese Committee on the Safety of Contrast Media. Radiology 175, 621-628.

Kavukcu, S., Soylu, A., Turkmen, M., 2002. The clinical value of urinary N-acetyl-beta-D-glucosaminidase levels in childhood age group. Acta Med. Okayama 56, 7-11.

Kaya, M., Gregory TS, 5., Dayton, P.A., 2009. Changes in lipid-encapsulated microbubble population during continuous infusion and methods to maintain consistency. Ultrasound Med. Biol. 35, 1748-1755.

Kinns, J., Aronson, L., Hauptman, J., Seiler, G., 2010. Contrast-enhanced ultrasound of the feline kidney. Vet. Radiol. Ultrasound 51, 168-172.

Kirchin, M.A., Pirovano, G., Venetianer, C., Spinazzi, A., 2001. Safety assessment of gadobenate dimeglumine (MultiHance): Extended clinical experience from phase I studies to post-marketing surveillance. J. Magn. Reson. Imaging 14, 281-294.

Kitano, M., Kudo, M., Maekawa, K., Suetomi, Y., Sakamoto, H., Fukuta, N., Nakaoka, R., Kawasaki, T., 2004. Dynamic imaging of pancreatic diseases by contrast enhanced coded phase inversion harmonic ultrasonography. Gut 53, 854-859.

Kitzman, D.W., Goldman, M.E., Gillam, L.D., Cohen, J.L., Aurigemma, G.P., Gottdiener, J.S., 2000. Efficacy and safety of the novel ultrasound contrast agent perflutren (Definity) in patients with suboptimal baseline left ventricular echocardiographic images. Am. J. Cardiol. 86, 669-674.

Kramer, K., Luft, U.C., 1951. Mobilization of red cells and oxygen from the spleen in severe hypoxia. Am. J. Physiol. 165, 215-228.

Kusnetzky, L.L., Khalid, A., Khumri, T.M., Moe, T.G., Jones, P.G., Main, M.L., 2008. Acute mortality in hospitalized patients undergoing echocardiography with and without an ultrasound contrast agent: Results in 18,671 consecutives. J. Am. Coll. Cardiol. 51, 1704-1706.

Kutara, K., Asano, K., Kito, A., Teshima, K., Kato, Y., Sasaki, Y., Edamura, K., Shibuya, H., Sato, T., Hasegawa, A., Tanaka, S., 2006. Contrast harmonic imaging of canine hepatic tumors. J. Vet. Med. Sci. 68, 433-438.

Lapointe, C., Belanger, M.C., Dunn, M., Moreau, M., Bedard, C., 2008. N-acetyl-beta-D-glucosaminidase index as an early biomarker for chronic kidney disease in cats with hyperthyroidism. J. Vet. Intern. Med. 22, 1103-1110.

LeBlanc, A.K., Daniel, G.B., 2007. Advanced imaging for veterinary cancer patients. Vet. Clin. North Am. Small Anim. Pract. 37, 1059-1077.

Lee, S.H., 2005. Contrast-enhanced ultrasonography of benign liver tumours. In: Albrecht, T., D'Onofrio, M., Frauscher, F. et al (Ed.), Contrast-Enhanced General Purpose Ultrasound. Springer-Verlag, Milan, 16-22.

Leen, E., 2001, USCAs. In: Goldberg, B.B, Raichlen, J.S., Forsberg, F. (Ed.), Ultrasound Contrast Agents. Basic Principles and Clinical Applications. Martin Dunitz Ltd., United Kingdom, 61-115.

Leen, E., Moug, S.J., Horgan, P., 2004. Potential impact and utilization of ultrasound contrast media. Eur. Radiol. 14, 16-24.

Lester, D., Greenberg, L.A., 1950. The Toxicity of sulfur hexafluoride. AIHOM 2, 348-349.

Levesque, M.J., Groom, A.C., 1976. Washout kinetics of red cells and plasma from the spleen. Am. J. Physiol. 231, 1665-1671.

Levesque, M.J., Groom, A.C., 1981. Fast transit of red cells and plasma in contracted versus relaxed spleens. Can. J. Physiol. Pharmacol. 59, 53-58.

Li, J., Dong, B., Yu, X., Wang, X., Li, C., 2005. Grey-scale contrast enhancement in rabbit liver with SonoVue at different doses. Ultrasound Med. Biol. 31, 185-190.

Li, J., Dong, B.W., Yu, X.L., Li, C.F., 2006. Gray scale contrast enhancement and quantification in different positions of rabbit liver. J. Ultrasound Med. 25, 7-14.

Li, N., Ding, H., Fan, P., Lin, X., Xu, C., Wang, W., Xu, Z., Wang, J., 2010. Intrahepatic transit time predicts liver fibrosis in patients with chronic hepatitis B: Quantitative assessment with contrast-enhanced ultrasonography. Ultrasound Med. Biol. 36, 1066-1075.

Liangos, O., Perianayagam, M.C., Vaidya, V.S., Han, W.K., Wald, R., Tighiouart, H., MacKinnon, R.W., Li, L., Balakrishnan, V.S., Pereira, B.J., Bonventre, J.V., Jaber, B.L., 2007. Urinary N-acetyl-beta-(D)-glucosaminidase activity and kidney injury molecule-1 level are associated with adverse outcomes in acute renal failure. J. Am. Soc. Nephrol. 18, 904-912.

Lim, A.K., Patel, N., Eckersley, R.J., Taylor-Robinson, S.D., Cosgrove, D.O., Blomley, M.J., 2004. Evidence for spleen-specific uptake of a microbubble contrast agent: A quantitative study in healthy volunteers. Radiology 231, 785-788.

Lucidarme, O., Franchi-Abella, S., Correas, J.M., Bridal, S.L., Kurtisovski, E., Berger, G., 2003. Blood flow quantification with contrast-enhanced US: "Entrance in the section" phenomenon--phantom and rabbit study. Radiology 228, 473-479.

Lueck, G.J., Kim, T.K., Burns, P.N., Martel, A.L., 2008. Hepatic perfusion imaging using factor analysis of contrast enhanced ultrasound. IEEE Trans. Med. Imaging 27, 1449-1457.

Main, M.L., 2009. Ultrasound contrast agent safety: from anecdote to evidence. J. Am. Coll. Cardiol. Cardiovasc. Imaging 2, 1057-1059.

Martegani, A., Aiani, L., Borghi, C., 2004. The use of contrast-enhanced ultrasound in large vessels. Eur. Radiol. 14, 73-86.

Matteucci, E., Gregori, G., Pellegrini, L., Navalesi, R., Giampietro, O., 1991. Effects of storage time and temperature on urinary enzymes. Clin. Chem. 37, 1436-1441.

Matteucci, E., Giampietro, O., 1994. To store urinary enzymes: How and how long? Kidney Int. 47, 58-59.

McCuskey, R.S., 2008. The hepatic microvascular system in health and its response to toxicants. Anat. Rec. 291, 661-671.

Mehran, R., Nikolsky, E., 2006. Contrast-induced nephropathy: Definition, epidemiology, and patients at risk. Kidney Int. 100, 11-15.

Metoki, R., Moriyasu, F., Kamiyama, N., Sugimoto, K., Iijima, H., Xu, H.X., Aoki, T., Miyata, Y., Yamamoto, K., Kudo, K., Shimizu, M., Yamada, M., 2006. Quantification of hepatic parenchymal blood flow by contrast ultrasonography with flash-replenishment imaging. Ultrasound Med. Biol. 32, 1459-1466.

Miller, D.L., Gies, R.A., 2000. The influence of ultrasound frequency and gas-body composition on the contrast agent-mediated enhancement of vascular bioeffects in mouse intestine. Ultrasound Med. Biol. 26, 307-313.

Miller, D.L., Dou, C., Wiggins, R.C., Wharram, B.L., Goyal, M., Williams, A.R., 2007. An in vivo rat model simulating imaging of human kidney by diagnostic ultrasound with gas-body contrast agent. Ultrasound Med. Biol. 33, 129-135.

Miller, D.L., Dou, C., Wiggins, R.C., 2008. Frequency dependence of kidney injury induced by contrast-aided diagnostic ultrasound in rats. Ultrasound Med. Biol. 34, 1678-1687.

Miller, D.L., Dou, C., Wiggins, R.C., 2009. Glomerular capillary hemorrhage induced in rats by diagnostic ultrasound with gas-body contrast agent produces intratubular obstruction. Ultrasound Med. Biol. 35, 869-877.

Miller, D.L., Dou, C., Wiggins, R.C., 2010. Contrast-enhanced diagnostic ultrasound causes renal tissue damage in a porcine model. J. Ultrasound Med. 29, 1391-1401.

Mitsuoka, Y., Hata, J., Haruma, K., Manabe, N., Tanaka, S., Chayama, K., 2007. New method of evaluating gastric mucosal blood flow by ultrasound. Scand. J. Gastroenterol. 42, 513-518.

Moran, C.M., Anderson, T., Sboros, V., Sutherland, G.R., Wright, R., McDicken, W.N., 1998. Quantification of the enhanced backscatter phenomenon from an intravenous and an intra-arterial contrast agent. Ultrasound Med. Biol. 24, 871-880.

Moran, C.M., Anderson, T., Pye, S.D., Sboros, V., McDicken, W.N., 2000. Quantification of microbubble destruction of three fluorocarbon-filled ultrasonic contrast agents. Ultrasound Med. Biol. 26, 629-639.

Moran, C.M., Watson, R.J., Fox, K.A., McDicken, W.N., 2002. In vitro acoustic characterisation of four intravenous ultrasonic contrast agents at 30 MHz. Ultrasound Med. Biol. 28, 785-791.

Morel, D.R., Schwieger, I., Hohn, L., Terrettaz, J., Llull, J.B., Cornioley, Y.A., Schneider, M., 2000. Human pharmacokinetics and safety evaluation of SonoVue, a new contrast agent for ultrasound imaging. Invest. Radiol. 35, 80-85.

Mueller, P.W., MacNeil, M.L., Steinberg, K.K., 1986. Stabilization of alanine aminopeptidase, gamma glutamyl transpeptidase, and N-acetyl-beta-D-glucosaminidase activity in normal urines. Arch. Environ. Contam. Toxicol. 15, 343-347.

Muir, W.W., 2007. Cardiovascular system. In: Tranquilli, W.J., Thurmon, J.C., Grimm, K.A. (Ed.), Lumb & Jones' Veterinary Anesthesia and Analgesia. Wiley-Blackwell, USA, 61-115.

Mulé, S., De Cesare, A., Lucidarme, O., Frouin, F., Herment, A., 2007. Tissue attenuation in small animals on contrast enhanced ultrasound. J. Radiol. 88, 1770-1776.

Mulé, S., De Cesare, A., Lucidarme, O., Frouin, F., Herment, A., 2008. Regularized estimation of contrast agent attenuation to improve the imaging of microbubbles in small animal studies. Ultrasound Med. Biol. 34, 938-948.

Mulvana, H., Stride, E., Hajnal, J.V., Eckersley, R.J., 2010. Temperature dependent behavior of ultrasound contrast agents. Ultrasound Med. Biol. 36, 925-934.

Nakamura, K., Sasaki, N., Yoshikawa, M., Ohta, H., Hwang, S.J., Mimura, T., Yamasaki, M., Takiguchi, M., 2009. Quantitative contrast-enhanced ultrasonography of canine spleen. Vet. Radiol. Ultrasound 50, 104-108.

Nakamura, K., Takagi, S., Sasaki, N., Kumara, W.R.B., Murakami, M., Ohta, H., Yamasaki, M., Takiguchi, M., 2010. Contrast-enhanced ultrasonography for characterization of canine focal liver lesions. Vet. Radiol. Ultrasound. 51, 79–85.

Nanda, N.C., Wistran, D.C., Karlsberg, R.P., Hack, T.C., Smith, W.B., Foley, D.A., Picard, M.H., Cotter, B., 2002. Multicenter evaluation of SonoVue for improved endocardial border delineation. Echocardiography 19, 27-36.

Narita, T., Tomizawa, N., Sato, R., Goryo, M., Hara, S., 2005. Effects of long-term oral administration of ketoprofen in clinically healthy beagle dogs. J. Vet. Med. Sci. 67, 847-853.

Nilsson, A., Olofsson, P.A., Loren, I., Carlstedt, L., Nilsson, P., 1997. Color Doppler energy: Computer analysis of color to assess angle dependency and detection of volume flow differences. J. Ultrasound Med. 16, 275-279.

Nilsson, A., 2004. Contrast-enhanced ultrasound of the kidneys. Eur. Radiol. 14, 104-109.

Nicolau, C., Catala, V., Vilana, R., Gilabert, R., Bianchi, L., Sole, M., Pages, M., Bru, C., 2004. Evaluation of hepatocellular carcinoma using SonoVue, a second generation ultrasound contrast agent: Correlation with cellular differentiation. Eur. Radiol. 14, 1092-1099.

Nyman, H.T., Kristensen, A.T., Kjelgaard-Hansen, M., McEvoy, F.J., 2005. Contrast-enhanced ultrasonography in normal canine liver. Evaluation of imaging and safety parameters. Vet. Radiol. Ultrasound 46, 243-250.

O'Brien, R.T., Iani, M., Matheson, J., Delaney, F., Young, K., 2004a. Contrast harmonic ultrasound of spontaneous liver nodules in 32 dogs. Vet. Radiol. Ultrasound 45, 547-553.

O'Brien, R.T., Waller, K.R., Osgood, T.L., 2004b. Sonographic features of drug-induced splenic congestion. Vet. Radiol. Ultrasound 45, 225-227.

O'Brien, R.T., 2007. Improved detection of metastatic hepatic hemangiosarcoma nodules with contrast ultrasound in three dogs. Vet. Radiol. Ultrasound 48, 146-148.

O'Brien, W.D.,Jr., Deng, C.X., Harris, G.R., Herman, B.A., Merritt, C.R., Sanghvi, N., Zachary, J.F., 2008. The risk of exposure to diagnostic ultrasound in postnatal subjects: Thermal effects. J. Ultrasound Med. 27, 517-535.

Ogura, T., Takaoka, M., Yamauchi, T., Oishi, T., Mimura, Y., Hashimoto, M., Asano, N., Yamamura, M., Otsuka, F., Makino, H., Ota, Z., Takahashi, K., 1996. Changes in urinary enzyme activity and histochemical findings in experimental tubular injury induced by gold sodium thiomalate. J. Med. 27, 41-55.

Ohlerth, S., Ruefli, E., Poirier, V., Roos, M., Kaser-Hotz, B., 2007a. Contrast harmonic imaging of the normal canine spleen. Vet. Radiol. Ultrasound 48, 451-456.

Ohlerth, S., Scharf, G., 2007b. Computed tomography in small animals - basic principles and state of the art applications. Vet. J. 173, 254-271.

Ohlerth, S., Dennler, M., Ruefli, E., Hauser, B., Poirier, V., Siebeck, N., Roos, M., Kaser-Hotz, B., 2008. Contrast harmonic imaging characterization of canine splenic lesions. J. Vet. Intern. Med. 22, 1095-1102.

Okada, M., Hoffmann, C.W., Wolf, K.J., Albrecht, T., 2005. Bolus versus continuous infusion of microbubble contrast agent for liver US: Initial experience. Radiology 237, 1063-1067.

Pace, G., Cowley, A., Campbell, A.M., 1997. Short pulse acoustic excitation of microbubbles. J. Acoust. Soc. Am. 102, 1474-1479.

Palacio, J., Liste, F., Gascon, M., 1997. Enzymuria as an index of renal damage in canine leishmaniasis. Vet. Rec. 140, 477-480.

Pallone, T.L., Silldorff, E.P., Turner, M.R., 1998. Intrarenal blood flow: Microvascular anatomy and the regulation of medullary perfusion. Clin. Exp. Pharmacol. Physiol. 25, 383-392.

Pallone, T.L., Zhang, Z., Rhinehart, K., 2003. Physiology of the renal medullary microcirculation. Am. J. Physiol. Renal Physiol. 284, 253-266.

Perazella, M.A., 2008. Gadolinium-contrast toxicity in patients with kidney disease: Nephrotoxicity and nephrogenic systemic fibrosis. Curr. Drug Saf. 3, 67-75.

Persson, A., Tepel, M., 2006. Contrast medium-induced nephropathy: The pathophysiology. Kindey Int. 100, 8-10.

Pey, P., Vignoli, M., Haers, H., Duchateau, L., Rossi, F., Saunders, J., 2010. Contrast-enhanced ultrasonography of the normal canine adrenal gland, congress abstract, EVDI Annual Scientific Conference, July 20th-24th, Giessen, Germany.

Pietra, M., Brini, E., Fracassi, F., Diana A., Cipone, M., 2005. Use of the galactose-based contrast agent SHU 508A (Levovist) in renal ultrasonography of the dog. Vet. Res. Commun. 29, 305-307.

Piscaglia, F., Bolondi, L., 2006. Italian Society for Ultrasound in Medicine and Biology (SIUMB) study group on ultrasound contrast agents, the safety of Sonovue in abdominal applications: Retrospective analysis of 23188 investigations. Ultrasound Med. Biol. 32, 1369-1375.

Pocsi, I., Taylor, S.A., Richardson, A.C., Aamlid, K.H., Smith, B.V., Price, R.G., 1990. "VRA-GlcNAc": Novel substrate for N-acetyl-beta-D-glucosaminidase applied to assay of this enzyme in urine. Clin. Chem. 36, 1884-1888.

Porter, T.R., Kricsfeld, D., Cheatham, S., Li, S., 1997. The effect of ultrasound frame rate on perfluorocarbon-exposed sonicated dextrose albumin microbubble size and concentration when insonifying at different flow rates, transducer frequencies, and acoustic outputs. J. Am. Soc. Echocardiog. 10, 593-601.

Potdevin, T.C., Fowlkes, J.B., Moskalik, A.P., Carson, P.L., 2006. Refill model of rabbit kidney vasculature. Ultrasound Med. Biol. 32, 1331-1338.

Prosperetti, A., 1991. The thermal behaviour of oscillating gas bubbles. J. Fluid. Mech. 222, 587-616.

Qin, S., Ferrara, K.W., 2007. The natural frequency of nonlinear oscillation of ultrasound contrast agents in microvessels. Ultrasound Med. Biol. 33, 1140-1148.

Quaia, E., Blomley, M.J., Patel, S., Harvey, C.J., Padhani, A., Price, P., Cosgrove, D.O., 2002. Initial observations on the effect of irradiation on the liver-specific uptake of Levovist. Eur. J. Radiol. 41, 192-199.

Quaia, E., Palumbo, A., Rossi, S., Degobbis, F., Cernic, S., Tona, G., Cova, M., 2006. Comparison of visual and quantitative analysis for characterization of insonated liver tumors after microbubble contrast injection. AJR Am. J. Roentgenol. 186, 1560-1570.

Raab, W.P., 1972. Diagnostic value of urinary enzyme determinations. Clin. Chem. 18, 5-25.

Rademacher, N., Ohlerth, S., Scharf, G., Laluhova, D., Sieber-Ruckstuhl, N., Alt, M., Roos, M., Grest, P., Kaser-Hotz, B., 2008. Contrast-enhanced power and color Doppler ultrasonography of the pancreas in healthy and diseased cats. J. Vet. Intern. Med. 22, 1310-1316.

Raekallio, M.R., Saario-Paunio, E.M., Rajamaki, M.M., Sankari, S.M., Palviainen, M.J., Siven, M.S., Peltoniemi, S.M., Leinonen, M.E., Honkavaara, J.M., Vainio, O.M., 2010. Early detection of ketoprofen-induced acute kidney injury in sheep as determined by evaluation of urinary enzyme activities. Am. J. Vet. Res. 71, 1246-1252.

Rahbin, N., Siösteen, A.K., Elvin, A., Blomqvist, L., Hagen, K., Hultcrantz, R., Aleman, S., 2008. Detection and characterization of focal liver lesions with contrast-enhanced ultrasonography in patients with hepatitis C-induced liver cirrhosis. Acta radiologica 49, 251-257.

Raichlen, J.S., 2001. Optimization of contrast echograms. In: Goldberg, B.B, Raichlen, J.S., Forsberg, F. (Ed.), Ultrasound Contrast Agents. Basic Principles and Clinical Applications. Martin Dunitz Ltd., United Kingdom, 131-142.

Rivers, B.J., Walter, P.A., O'Brien, T.D., King, V.L., Polzin, D.J., 1996. Evaluation of urine gamma-glutamyl transpeptidase-to-creatinine ratio as a diagnostic tool in an experimental model of aminoglycoside-induced acute renal failure in the dog. J. Am. Anim. Hosp. Assoc. 32, 323-336.

Rognin, N.G., Frinking, P., Costa, M., Arditi, M., 2008. In-vivo perfusion quantification by contrast ultrasound: Validation of the use of linearized video data vs. raw RF data. IEEE International Ultrasonics Symposium Proceedings, 1690-1693.

Rosenberg, M.L., Carpenter, A.P., Phase III Definity clinical investigators, 2002. Contrast material-enhanced abdominal US examinations with DMP 115 (Definity) provides additional diagnostic information with potential for changes in patient management. Acad. Radiol. 9, 243-245.

Rossi, F., Leone, V.F., Vignoli, M., Laddaga, E., Terragni, R., 2008. Use of contrast-enhanced ultrasound for characterization of focal splenic lesions. Vet. Radiol. Ultrasound 49, 154-164.

Rossi, F., Rabba, S., Vignoli, M., Haers, H., Terragni, R., Saunders, J.H., 2010. B-mode and contrast-enhanced sonographic assessment of accessory spleen in the dog, Vet. Radiol. Ultrasound 51, 173-177.

Rubaltelli, L., Khadivi, Y., Tregnaghi, A., Stramare, R., Ferro, F., Borsato, S., Fiocco, U., Adami, F., Rossi, C.R., 2004. Evaluation of lymph node perfusion using continuous mode harmonic ultrasonography with a second-generation contrast agent. J. Ultrasound Med. 23, 829-836.

Rubin, J.M., Bude, O., Carson, P.L., Bree, R.L., Adler, R.S., 1994. Power Doppler US: A potentially useful alternative to mean frequency-based color Doppler US. Radiology 190, 853-856.

Russo, M., Vignoli, M., Catone, G., Rossi, F., Attanasi, G., England, G.C., 2009. Prostatic perfusion in the dog using contrast-enhanced Doppler ultrasound. Reprod. Domest. Anim. 44, 334-335.

Salwei, R.M., O'Brien, R.T., Matheson, J.S., 2005. Characterization of lymphomatous lymph nodes in dogs using contrast harmonic and power Doppler ultrasound. Vet. Radiol. Ultrasound 46, 411-416.

Sato, R., Soeta, S., Miyazaki, M., Syuto, B., Sato, J., Miyake, Y., Yasuda, J., Okada, K., Naito, Y., 2002a. Clinical availability of urinary N-acetyl-beta-D-glucosaminidase index in dogs with urinary diseases. J. Vet. Med. Sci. 64, 361-365.

Sato, R., Soeta, S., Syuto, B., Yamagishi, N., Sato, J., Naito, Y., 2002b. Urinary excretion of N-acetyl-beta-D-glucosaminidase and its isoenzymes in cats with urinary isease. J. Vet. Med. Sci. 64, 367-371.

Sboros, V., Moran, C.M., Pye, S.D., McDicken, W.N., 2003. The behaviour of individual contrast agent microbubbles. Ultrasound Med. Biol. 29, 687-694.

Schaser, K.D., Puhl, G., Vollmar, B., Menger, M.D., Stover, J.F., Kohler, K., Neuhaus, P., Settmacher, U., 2005. In vivo imaging of human pancreatic microcirculation and pancreatic tissue injury in clinical pancreas transplantation. Am. J. Transplant. 5, 341-350.

Schiller, W.R., Anderson, M.C., 1975. Microcirculation of the normal and inflamed canine pancreas. Ann. Surg. 181, 466-470.

Schlosser, T., Pohl, C., Veltmann, C., Lohmaier, S., Goenechea, J., Ehlgen, A., Köster, J., Bimmel, D., Kuntz-Hehner, S., Becher, H., Tiemann, K., 2001. Feasibility of the flash-replenishment concept in renal tissue: Which parameters affect the assessment of the contrast replenishment? Ultrasound Med. Biol. 27, 937-944.

Schmidt, E.E., MacDonald, I.C., Groom, A.C., 1982. Direct arteriovenous connections and the intermediate circulation in dog spleen, studied by scanning electron microscopy of microcorrosion casts. Cell Tissue Res. 225, 543-555.

Schmidt, E.E., MacDonald, I.C., Groom, A.C., 1983. The intermediate circulation in the nonsinusal spleen of the cat, studied by scanning electron microscopy of microcorrosion casts. J. Morphol. 178, 125-138.

Schrope, B.A., Newhouse, V.L., 1993. Second harmonic ultrasonic blood perfusion measurement. Ultrasound Med. Biol. 19, 567-579.

Schummer, A., Wilkens, H., Vollmerhaus B., Habermehl, K.H., 1979. Urogenital system. In: Nickel, R., Schummer, A., Seiferle, E., (Ed.), The Viscera of the Domestic Mammals Vol. 2. Springer-Verlag.USA, 287, 291-292.

Schummer, A., Wilkens, H., Vollmerhaus, B., Habermehl, K.H., 1981a. Arteries (Arteriae). Veins (Venae). In: Nickel, R., Schummer, A., Seiferle, E., (Ed.), The Anatomy of the Domestic Animals Vol. 3 The Circulatory System, the Skin, and the Cutaneous Organs of the Domestic Mammals. Springer-Verlag. USA, 161-162, 168-170, 175-176.

Schummer, A., Wilkens, H., Vollmerhaus, B., Habermehl, K.H., 1981b. Veins (Venae). Veins (Venae). In: Nickel R., Schummer A., Seiferle E., (Ed.), The Anatomy of the Domestic Animals Vol. 3 The Circulatory System, the Skin, and the Cutaneous Organs of the Domestic Mammals. Springer-Verlag. USA, 260-265, 361.

Seidel, G., Algermissen, C., Christoph, A., Claassen, L., Vidal-Langwasser, M., Katzer, T., 2000. Harmonic imaging of the human brain. Visualization of brain perfusion with ultrasound. Stroke 31, 151-154.

Seidel, G., Meairs, S., 2009. Ultrasound contrast agents in ischemic stroke. Cerebrovasc. Dis. 27, 25-39.

Simpson, D.H., Chin, C.T., Burns, P.N., 1999. Pulse inversion Doppler: A new method for detecting nonlinear echoes from microbubble contrast agents. IEEE Trans. Ultrason. Ferroelec. Freq. Contr. 46, 372-382.

Skyba, D.M., Jayaweera, A.R., Goodman, N.C., Ismail, S., Camarano, G., Kaul, S., 1994. Quantification of myocardial perfusion with myocardial contrast echocardiography during left atrial injection of contrast. Implications for venous injection. Circulation 90, 1513-1521.

Solbiati, L., Ierace, T., Tonolini, M., Cova, L., 2004. Guidance and monitoring of radiofrequency liver tumor ablation with contrast-enhanced ultrasound. Eur. J. Radiol. 14, 19-23.

Song, S.H., Groom, A.C., 1971. Storage of blood cells in spleen of the cat. Am. J. Physiol. 220, 779-784.

Sonne, C., Xie, F., Lof, J., Oberdorfer, J., Phillips, P., Carr Everbach, E., Porter, T.R., 2003. Differences in Definity and Optison microbubble destruction rates at a similar mechanical index with different real-time perfusion systems. J. Am. Soc. Echocardiog. 16, 1178-1185.

Su, H.L., Qian, Y.Q., Wei, Z.R., He, J.G., Li, G.Q., Zhang, J., Zhou, X.D., Jing, W., 2009. Real-time myocardial contrast echocardiography in rat: Infusion versus bolus administration. Ultrasound Med. Biol. 35, 748-755.

Talu, E., Powell, R.L., Longo, M.L., Dayton, P.A., 2008. Needle size and injection rate impact microbubble contrast agent population. Ultrasound Med. Biol. 34, 1182-1185.

Tang, M.X., Eckersley, R.J., 2007. Frequency and pressure dependent attenuation and scattering by microbubbles. Ultrasound Med. Biol. 33, 164-168.

Tang, M.X., Kamiyama, N., Eckersley, R.J., 2010. Effects of nonlinear propagation in ultrasound contrast agent imaging. Ultrasound Med. Biol. 36, 459-466.

Taylor, G.A., Ecklund, K., Dunning, P.S., 1996. Renal cortical perfusion in rabbits: Visualization with color amplitude imaging and an experimental microbubble-based US contrast agent. Radiology 201, 125-129.

Taylor, G.A., Barnewolt, C.E., Claudon, M., Dunning, P.S., 1999. Depiction of renal perfusion defects with contrast-enhanced harmonic sonography in a porcine model. AJR Am. J. Roentgenol. 173, 757-760.

Thomas, D.H., Butler, M.B., Anderson, T., Steel, R., Pye, S.D., Poland, M., Brock-Fisher, T., McDicken,W.N., Sboros, V., 2009. Single microbubble response using pulse sequences: Initial results. Ultrasound Med. Biol. 35, 112-119.

Thorelius, L., 2004. Contrast-enhanced ultrasound in trauma. Eur. Radiol. 14, 43-52.

Trachtenberg, F., Barregard, L., 2007. The effect of age, sex, and race on urinary markers of kidney damage in children. Am. J. Kidney Dis. 50, 938-945.

Trof, R.J., Di Maggio, F., Leemreis, J., Groeneveld, A.B., 2006. Biomarkers of acute renal injury and renal failure. Shock 26, 245-253.

Uechi, M., Nogami, Y., Terui, H., Nakayama, T., Ishikawa, R., Wakao, Y., Takahashi, M., 1994a. Evaluation of urinary enzymes in dogs with early renal disorder. J. Vet. Med. Sci. 56, 555-556.

Uechi, M., Terui, H., Nakayama, T., Mishina, M., Wakao, Y., Takahashi, M., 1994b. Circadian variation of urinary enzymes in the dog. J. Vet. Med. Sci. 56, 849-854.

Uechi, M., Uechi, H., Nakayama, T., Wakao, Y., Ogasawara, T., Takase, K., Takahashi, M., 1998. The circadian variation of urinary N-acetyl-beta-D-glucosaminidase and gamma-glutamyl transpeptidase in clinically healthy cats. J. Vet. Med. Sci. 60, 1033-1034.

Uhlendorf, V., 1994. Physics of ultrasound contrast imaging: Scattering in the linear range. IEEE Trans. Ultrason. Ferroelec. Freq. Contr. 41, 70-79.

Uhlendorf, V., Scholle, F.D., Reinhardt, M., 2000. Acoustic behaviour of current ultrasound contrast agents. Ultrasonics 38, 81-86.

Van Camp, G., Droogmans, S., Cosyns, B., 2007. Bio-effects of ultrasound contrast agents in daily clinical practice: Fact or fiction? Eur. Heart J. 28, 1190-1192.

Van der Meer, S.M., Dollet, B., Voormolen, M.M, Chin, C.T., Bouakaz, A., de Jong, N., Versluis, M., Lohse, D., 2007. Microbubble spectroscopy of ultrasound contrast agents. J. Acoust. Soc. Am. 121, 648-656.

Van Liew, H.D., Burkard, M.E., 1995. Bubbles in circulating blood: Stabilization and simulations of cyclic changes of size and content. J. Appl. Physiol. 79, 1379-1385.

Verbeek, X.A., Willigers, J.M., Prinzen, F.W., Peschar, M., Ledoux, L.A., Hoeks, A.P., 2001. High-resolution functional imaging with ultrasound contrast agents based on RF processing in an in vivo kidney experiment. Ultrasound Med. Biol. 27, 223-233.

Vignoli, M., Russo, M., Catone, G., Rossi, F., Attanasi, G., Terragni, R., Saunders, J.H., England, G.C., 2010. Assessment of vascular perfusion kinetics using contrast-enhanced ultrasound for the diagnosis of prostatic disease in dogs. Reprod. Domest. Anim., in press.

Villa, A., Van Steenwinkel, C., Meloni, G., Campani, R., 1995. Dynamic contrast enhanacement in magnetic resonance imaging of the body. In: Rinck, P.A. (Ed.), The Rational Use of Magnetic Resonance Imaging. Blackwell Wissenschafts-Verlag, Berlin, 257-278.

Volta, A., Manfredi, S., Gnudi, G., Bigliardi, E., Cantoni, A.M., Bertoni, G., 2010. Contrast-enhanced ultrasonographic features of testicular lesions in dogs, congress abstract, EVDI Annual Scientific Conference, July 20th-24th, Giessen, Germany.

Waller, K.R., O'Brien, R.T., Zagzebski, J.A., 2007. Quantitative contrast ultrasound analysis of renal perfusion in normal dogs. Vet. Radiol. Ultrasound 48, 373-377.

Wang, Z., Tang, J., An, L., Wang, W., Luo,Y., Li, J., Xu,J., 2007. Contrast-enhanced ultrasonography for assessment of tumor vascularity in hepatocellular carcinoma. J.Ultrasound Med. 26, 757-762.

Ward, B., Baker, A.C., Humphrey, V.F., 1997. Nonlinear propagation applied to the improvement of resolution in diagnostic medical ultrasound. J. Acoust. Soc. Am. 101, 143-154.

Watson, A.D., Church, D.B., Fairburn, A.J., 1981. Postprandial changes in plasma urea and creatinine concentrations in dogs. Am. J. Vet. Res. 42, 1878-1880.

Wei, K., 2001. Blood flow and perfusion measurements: Background and clinical utility. In: Goldberg, B.B, Raichlen, J.S., Forsberg, F. (Ed.), Ultrasound Contrast Agents. Basic Principles and Clinical Applications. Martin Dunitz Ltd., United Kingdom, 90-104.

Westhuyzen, J., Endre, Z.H., Reece, G., Reith, D.M., Saltissi, D., Morgan, T.J., 2003. Measurement of tubular enzymuria facilitates early detection of acute renal impairment in the intensive care unit. Nephrol. Dial. Transplant. 18, 543-551.

Wheatley, M.A., Schrope, B., Shen, P., 1990. Contrast agents for diagnostic ultrasound: Development and evaluation of polymer-coated microbubbles. Biomaterials 11, 713-717.

Wheatley, M.A., 2001. Composition of contrast microbubbles: Basic chemistry of encapsulated and surfactant-coated bubbles. In: Goldberg, B.B, Raichlen, J.S., Forsberg, F. (Ed.), Ultrasound Contrast Agents. Basic Principles and Clinical Applications. Martin Dunitz Ltd., United Kingdom, 3-14.

Whittingham, T.A., 2007. WFUMB safety symposium on echo-contrast agents: Exposure from diagnostic ultrasound equipment relating to cavitation risk. Ultrasound Med. Biol. 33, 214-223.

Wible, J.H.Jr., Galen, K.P., Wojdyla, J.K., Hughes, M.S., Klibanov, A.L., Brandenburger, G.H., 2002. Microbubbles induce renal hemorrhage when exposed to diagnostic ultrasound in anesthetized rats. Ultrasound Med. Biol. 28, 1535-1546.

Williams, A.R., Wiggins, R.C., Wharram, B.L., Goyal, M., Dou, C., Johnson, K.J., Miller, D.L., 2007. Nephron injury induced by diagnostic ultrasound imaging at high mechanical index with gas body contrast agent. Ultrasound Med. Biol. 33, 1336-1344.

Wilson, D.V., Evans, A.T., Carpenter, R.A., Mullineaux, D.R., 2004. The effect of four anesthetic protocols on splenic size in dogs. Vet. Anaesth. Analg. 31, 102-108.

Wilson, S.R., Jang, H.J., Kim, T.K., Burns, P.N., 2007. Diagnosis of focal liver masses on ultrasonography: Comparison of unenhanced and contrast-enhanced scans. J. Ultrasound Med. 26, 775-787.

Wouters, P.F., Van de Velde, M.A., Marcus, M.A., Deruyter, H.A., Van Aken, H., 1995. Hemodynamic changes during induction of anesthesia with eltanolone and propofol in dogs. Anesth. Analg. 81, 125-131.

Wu, J., Tong, J., 1998. Measurements of the nonlinearity parameter B/A of contrast agents. Ultrasound Med. Biol. 24, 153-159.

Yanagisawa, K., Moriyasu, F., Miyahara, T., Yuki, M., Iijima, H., 2007. Phagocytosis of ultrasound contrast agent microbubbles by Kupffer cells. Ultrasound Med. Biol. 33, 318-25.

Yeh, C.K., Su, S.Y., 2008. Effects of acoustic insonation parameters on ultrasound contrast agent destruction. Ultrasound Med. Biol. 34, 1281-1291.

Zhu, T., Pang, Q., McCluskey, S.A., Luo, C., 2008. Effect of propofol on hepatic blood flow and oxygen balance in rabbits. Can. J. Anaesth. 55, 364-370.

Ziegler, L.E., O'Brien, R.T., Waller, K.R., Zagzebski, J.A., 2003. Quantitative contrast harmonic ultrasound imaging of normal canine liver. Vet. Radiol. Ultrasound 44, 451-454.